Journal of Computational Physics 231 (2012) 7608–7625

Contents lists available at SciVerse ScienceDirect

Journal of Computational Physics

journal homepage: www.elsevier.com/locate/jcp

Accurate absorbing boundary conditions for anisotropic elastic media. Part 2: Untilted non-elliptic anisotropy

Siddharth Savadatti, Murthy N. Guddati *

Department of Civil, Construction and Environmental Engineering, North Carolina State University, Raleigh, NC 27695-7908, United States

ARTICLE INFO

Article history:
Received 1 September 2011
Received in revised form 29 March 2012
Accepted 29 May 2012
Available online 26 June 2012

Keywords:
Wave propagation
Perfectly matched layers
Group velocity
Rational approximation

ABSTRACT

With the ultimate goal of devising effective absorbing boundary conditions (ABCs) for general elastic media, we investigate the accuracy aspects of local ABCs designed for untilted non-elliptic anisotropy in the frequency domain (time-harmonic analysis). While simple space–time transformations are available to treat the wavemodes with opposing phase and group velocities present in elliptic anisotropic media, no such transformations are known to exist for the case of non-elliptic anisotropy. In this paper, we use the concept of layer groupings along with an unconventional stretching of the finite element mesh to guarantee the accuracy of local ABCs designed to treat all propagating wavemodes, even those with opposing phase and group velocities. The local ABC used here is the perfectly matched discrete layer (PMDL) which is a simple variant of perfectly matched layers (PMLs) that is also equivalent to rational approximation-based local ABCs (rational ABCs); it inherits the straightforward approximation properties of rational ABCs along with the versatility of PML. The approximation properties of PMDL quantified through its reflection matrix allow us to (a) show that it is impossible to design an accurate PMDL with wavenumber-independent parameters, (b) theoretically demonstrate the ability of wavenumber-dependent parameters to ensure accuracy, and finally (c) design a practical though unconventional stretching of the finite element PMDL mesh that facilitates the implementation of wavenumber-dependent parameters. The validity of this work is demonstrated through a series of numerical experiments.

1. Introduction

Absorbing boundary conditions (ABCs) have long been used to include the effect of 'exterior' unbounded domains on computational models of finite 'interiors' at the 'computational boundary' (boundary between exterior and interior). Time-harmonic modeling of such domains requires the ABCs to *accurately* represent the unbounded exterior effect i.e. the ABC should absorb *all* outgoing waves at the computational boundary.

Exact ABCs, though ideal, are not always available for complex anisotropic and/or heterogeneous media and hence approximate ABCs are used in these cases. Approximate ABCs can be divided into global and local ABCs; global ABCs are prohibitively expensive for large scale simulations and hence the more efficient though less accurate local ABCs are preferred. The most popular local ABCs currently available are rational approximation based ABCs (rational ABCs) and perfectly matched layers (PMLs). Earlier formulations of rational ABCs and PML can be found in [1–10] with later extensions and advancements being presented in [11–21].

* Corresponding author. Tel.: +1 (919) 515 7699; fax: +1 (919) 515 7908.
E-mail address: murthy.guddati@ncsu.edu (M.N. Guddati).

0021-9991/$ - see front matter © 2012 Elsevier Inc. All rights reserved.
http://dx.doi.org/10.1016/j.jcp.2012.05.039

Though based on disparate ideas, rational ABCs and PML are now known to share underlying links that have made it possible to view certain rational ABCs as modified versions of PML [22]. One such local ABC is the perfectly matched *discrete* layer (PMDL) that inherits the versatility of PML along with the more transparent approximation characteristics of rational ABCs [23]. Since PMDL can be viewed as either rational ABCs or as PML, we have the convenience of choosing the viewpoint that best facilitates the study at hand. While some studies on the accuracy and well-posedness of PMDL for anisotropic acoustics are based primarily on the rational ABC viewpoint [24,25], other studies like the prequel to this paper on the accuracy of PMDL for elliptic anisotropic elasticity have been based primarily on the PML viewpoint [26]. In this work we look at PMDL mainly through the rational ABC viewpoint by examining its reflection coefficient.

The PML works primarily on the concept of mimicking the exterior wave absorption characteristics by enforcing wave amplitude decay. Its superiority over other absorbing media can be attributed to its 'perfect matching' property that allows (in theory) a reflectionless transmission of waves across the computational boundary. The rate and sign of decay depends on the phase velocity of the outgoing wavemodes (those leaving the interior) with certain phase velocities (say positive) leading to decay and consequently other (negative) phase velocities leading to growth. Hence PML acts as an absorber as long as the outgoing wavemodes have positive phase velocities. Since wavemodes are categorized into outgoing and incoming wavemodes based on the sign of their group velocity (positive and negative respectively), PML acts as an absorber as long as the phase (c_{px}) and group (c_{gx}) velocity signs match i.e. as long as $c_{px}c_{gx} \geqslant 0$. However, there exist many anisotropic and/or heterogeneous media that support wavemodes with $c_{px}c_{gx} < 0$. For such media, PML results in amplitude growth (not decay) and such growth ends up mimicking energy input instead of energy absorption.

Space–time transformations that result in a transformed space with $c_{px}c_{gx} \geqslant 0$ are the most frequently used method for tackling issues related to $c_{px}c_{gx} < 0$ [27–30]. While easy to understand, space–time transformations have two major drawbacks: their extension to heterogeneous (layered) media is unclear and their applicability is restricted to *elliptic* anisotropy. The predecessor to this paper [26] dealt with the first drawback by providing a solution for *elliptic* anisotropic elasticity *without* the use of space–time transformations thus making the solution more amenable to extensions involving heterogeneous (layered) media. In this part, we address the case of *non-elliptic anisotropy* and design an unconventional mesh stretching idea that ensures the accurate absorption of propagating wavemodes.

The purpose of this paper is limited to providing a local ABC that accurately treats the propagating wavemodes of untilted non-elliptic anisotropic elasticity in the frequency domain. However, accuracy in the frequency domain is intricately linked to accuracy, wellposedness and stability in the time domain e.g. local ABCs that allow incoming propagating modes are known to be ill-posed or unstable in the time domain and the same ABCs end up being inaccurate in the frequency domain because incoming modes are equivalent to spurious reflections at the computational boundary. Though inaccuracies and instabilities tied to the existence of modes with $c_{px}c_{gx} < 0$ have been studied extensively [14,19,28–41], we wish to assert that there exists no solution – to the best of our knowledge – that rigorously ensures accurate absorption of wavemodes with $c_{px}c_{gx} < 0$ present in *non-elliptic* anisotropic elasticity (both untilted and tilted). This paper provides an accurate ABC for the untilted case. It should be pointed out that there do exist ways of ensuring stability for non-elliptic anisotropy e.g. [14,15,41–44]. However, these studies do not seem to tackle directly the issue of $c_{px}c_{gx} < 0$ and their precise effect on the inaccuracies and instabilities created by wavemodes with $c_{px}c_{gx} < 0$ is not clear.

We design an accurate local ABC for untilted non-elliptic anisotropic elasticity based on PMDL. Using the reflection matrix, we first specify a sequence of successively weak sufficient conditions by utilizing the concept of layer groupings. We next show that it is impossible for a traditional PMDL with wavenumber-independent parameters to meet any of these sufficient conditions. This is followed by a proof that reveals the accuracy of a PMDL with wavenumber-dependent parameters. We finally present an unconventional stretching of the PMDL mesh that facilitates the implementation of these wavenumber-dependent parameters.

This paper borrows heavily from its predecessor [26] and familiarity with the basic notation is assumed (even though some of the equations are repeated for clarity). Also, this paper is only concerned with the accuracy issues of propagating wavemodes in the frequency domain analysis of the continuous problem with a straight computational boundary. As such, interior discretization errors, corners, curved computational boundaries, and inaccuracies due to the neglect of evanescent wavemodes are outside the scope of this paper. It should be noted that the above restrictions are imposed to make the analysis of the method more tractable; they are, with the exception of curved boundaries, not due to any limitations of the PMDL formulation. PMDLs capable of absorbing both propagating and evanescent waves have already been implemented on domains with convex polygonal corners in [45]. As such, this paper can be considered as a necessary step towards a complete PMDL implementation for anisotropic elastic media. Analogous studies for time-harmonic *and* transient modeling of antiplane shear waves can be found in [24,25].

The outline of the rest of the paper is as follows. Section 2 provides a summary of the main results. Section 3 contains preliminaries mostly summarized from [26]. In Section 4 we present the criterion for accuracy along with a sequence of sufficient conditions followed by two necessary conditions based on the concept of layer groupings. Section 5 proves that it is impossible to design an accurate PMDL for propagating wavemodes with wavenumber-independent parameters. It also contains the derivation of wavenumber-dependent PMDL parameters that ensure the accurate treatment of propagating modes, followed by an unconventional stretching of the PMDL mesh that facilitates implementation. Various numerical experiments are presented in Section 6 and finally, Section 7 contains a summary and conclusions.

2. Summary of procedure and main result

In part 1 [26], for the case of *elliptic* anisotropic media, we showed that the reflections inherent in truncated ABCs can be utilized to ensure accuracy even in the presence of growth of outgoing wavemodes with negative phase velocities. It turns out that this methodology cannot be extended to the case of untilted *non-elliptic* anisotropy because of the presence of discontinuities in the outgoing/incoming branches of the slowness diagram (thick/thin lines in Fig. 1b). In this paper, we show that these discontinuities preclude the use of traditional ABCs with wavenumber independent layer lengths; in fact, they necessitate an even number of PMDL layers with wavenumber *dependent* lengths paired in such a way that they capture only the right branch of the slowness diagram (thick lines in Fig. 1b). Furthermore, it is shown that such layer-pairing is equivalent to an unconventionally stretched $2n$-layer PMDL mesh shown in Fig. 1a, which is straightforward to implement.

To be precise, in a full-space made up of an elastic material with untilted non-elliptic anisotropy, the effect of the exterior right half-space on propagating wavemodes can be accurately captured at the computational boundary by using an ABC made up of an unconventionally stretched mesh of '$2n$' PMDL layers shown in Fig. 1a. The mesh consists of n groups of 2 layers each with the two layers in each group having the same length but opposite (negative) stretch. The layer lengths and associated stretches for each of the n groups are obtained using a simple algorithm:

Choose $\sigma^*_{y,j} \in [\sigma_{y0}, \sigma_{y1}], \quad j = 1 \ldots n.$

Compute $\sigma_{xo,j} = \sigma_{x1}|_{\sigma_y=\pm\sigma_{y2}} \Big/ \sqrt{\left(\sigma_{y2}/\sigma^*_{y,j}\right)^2 - 1}.$

Obtain layer parameters, $L_j = 2i/\omega\sigma_{xo,j}, \quad \theta_j = \tan^{-1}\left(\sigma_{xo,j}/\sigma^*_{y,j}\right).$

In the above, $\sigma_{x1}|_{\sigma_y=\pm\sigma_{y2}}, \sigma_{y0}, \sigma_{y1}, \sigma_{y2}$ are obtained from the full slowness diagrams shown in Fig. 1b–c. The layer lengths shown in Fig. 1a are $L'_j = L_j/\cos\theta_j$.

3. Preliminaries

This section borrows heavily from the corresponding section of part 1 [26].

3.1. Model problem and anisotropic elasticity

The model problem consists of replacing an exact full-space by a left half-space (interior) along with an ABC that simulates the effect of the right half-space (exterior) at the computational boundary ($x = 0$) as shown in Fig. 2 (left). The time-harmonic vector wave equation representing in-plane wave motions in homogeneous anisotropic elastic media is,

$$\left(\mathbf{G}_{xx}\frac{\partial^2}{\partial x^2} + \left(\mathbf{G}_{xy} + \mathbf{G}^T_{xy}\right)\frac{\partial^2}{\partial x \partial y} + \mathbf{G}_{yy}\frac{\partial^2}{\partial y^2} + \omega^2\mathbf{I}\right)\mathbf{u} = \mathbf{0}, \tag{1}$$

where $\omega \in \mathbb{R}$ is the temporal frequency, $\mathbf{u} = \{u_x \; u_y\}^T$ is the infinitesimal in-plane displacement vector and $\mathbf{G}_{xx}$, $\mathbf{G}_{yy}$, $\mathbf{G}_{xy}$ are the in-plane matrix coefficients given by,

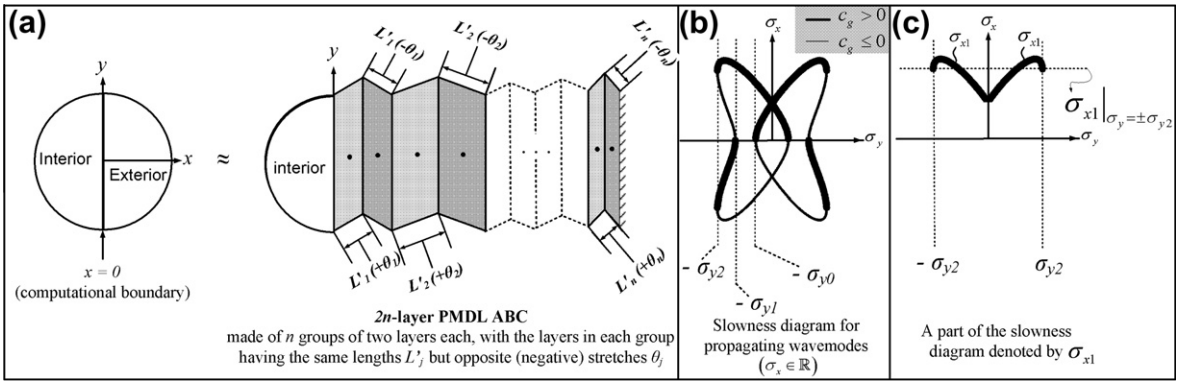

Fig. 1. (a) Model problem of approximating the effect of a right half-space by an unconventionally stretched $2n$-layer PMDL ABC; (b) Slowness diagram for propagating wavemodes ($\sigma_x \in \mathbb{R}$) with horizontal slownesses supported by right and left half-spaces demarcated by bold ($c_g > 0$) and thin lines ($c_g \leqslant 0$) respectively and certain specific vertical slownesses σ_{y0}, σ_{y1}, σ_{y2} shown; and (c) Part of the slowness diagram supported by the right half-space denoted by σ_{x1}.

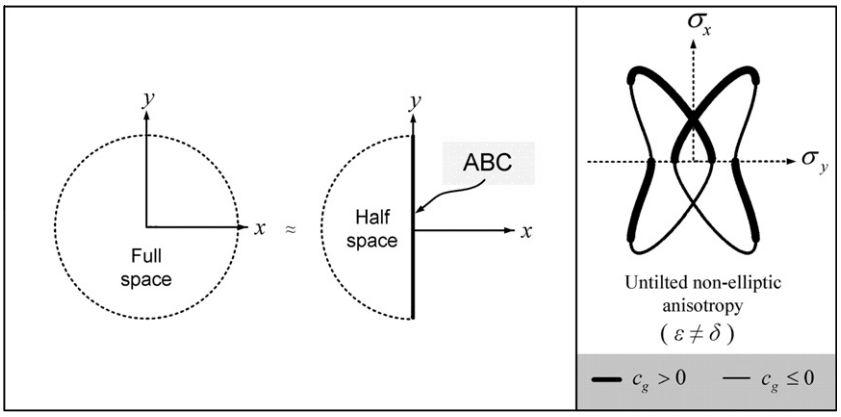

Fig. 2. *Left:* The model problem consists of replacing a full space of untilted non-elliptic anisotropic elastic media by a left half-space and an efficient ABC that accurately mimics the behavior of the right half-space. *Right:* Slowness diagram for in-plane propagating ($\sigma_x \in \mathbb{R}$) wavemodes in untilted non-elliptic anisotropic elasticity. Since $c_{px} = 1/\sigma_x$, parts of the curve with $c_{gx} < 0$ ($c_{gx} > 0$) in the upper (lower) half plane represent wavemodes with $c_{px}c_{gx} < 0$.

$$\mathbf{G}_{xx} = \begin{bmatrix} (1+2\varepsilon)c_p^2 & 0 \\ 0 & c_s^2 \end{bmatrix}, \quad \mathbf{G}_{yy} = \begin{bmatrix} c_s^2 & 0 \\ 0 & c_p^2 \end{bmatrix}, \quad \mathbf{G}_{xy} = \begin{bmatrix} 0 & \sqrt{\left((1+2\delta)c_p^2 - c_s^2\right)\left(c_p^2 - c_s^2\right)} - c_s^2 \\ c_s^2 & 0 \end{bmatrix}. \tag{2}$$

In (2), c_p is the pressure wave velocity, c_s is the shear wave velocity ($c_P \geqslant c_s$), and ε, δ are the parameters of anisotropy [17,46]. The above refers to an *untilted* material i.e. one whose principal material axis is aligned with the coordinate axis ($\beta = 0$ in [26]). For the sake of presentation, we Fourier transform (1) in y to obtain the reduced equation with the duality $\partial/\partial y \leftrightarrow ik_y$,

$$\left(\mathbf{G}_{xx}\frac{\partial^2}{\partial x^2} + ik_y\left(\mathbf{G}_{xy} + \mathbf{G}_{xy}^T\right)\frac{\partial}{\partial x} - \left(k_y^2\mathbf{G}_{yy} - \omega^2\mathbf{I}\right)\right)\mathbf{u} = \mathbf{0}. \tag{3}$$

Eq. (3) admits individual *normalized* ($\|\cdot\| = 1$) modes of the kind $\mathbf{a}e^{ik_x x}$ which, in the general case are defined by their wavenumber-wavemode pair $(k_x, \mathbf{a})$ *for a given* $(k_y, \omega) \in \mathbb{R}^2$. The dispersion relation is given by $\det\left(\mathbf{\Lambda}^{in}\right) = 0$ where,

$$\mathbf{\Lambda}^{in} \equiv \left(k_x^2\mathbf{G}_{xx} + k_x k_y\left(\mathbf{G}_{xy} + \mathbf{G}_{xy}^T\right) + k_y^2\mathbf{G}_{yy} - \omega^2\mathbf{I}\right). \tag{4}$$

Plots of $\det\left(\mathbf{\Lambda}^{in}\right) = 0$ are viewed through slowness diagrams (plots of $\sigma_x = k_x/\omega$ vs. $\sigma_y = k_y/\omega$) with the case of non-elliptic anisotropy ($\varepsilon \neq \delta$) exhibiting modes with $c_{px}c_{gx} < 0$ as shown in Fig. 2(right). Note that in Fig. 2(right), the part of the slowness diagram in the upper half plane ($1/c_{px} = \sigma_x > 0$) represents wavemodes with positive phase velocities and the part of the slowness diagrams marked with a thick line have positive group velocities. Propagating ($k_x \in \mathbb{R}$) and evanescent wavemodes ($k_x \notin \mathbb{R}$) can be characterized into outgoing or incoming wavemodes as follows:

$$\left.\begin{array}{ll} \text{forward propagating}: & \Im m(k_x) = 0 \quad \text{and} \quad c_{gx} = \frac{\partial\omega}{\partial k_x} > 0, \\ \text{forward decaying}: & \Im m(k_x) > 0, \end{array}\right\} \text{outgoing modes}, \tag{5}$$

$$\left.\begin{array}{ll} \text{backward propagating}: & \Im m(k_x) = 0 \quad \text{and} \quad c_{gx} = \frac{\partial\omega}{\partial k_x} \leqslant 0, \\ \text{backward decaying}: & \Im m(k_x) < 0. \end{array}\right\} \text{incoming modes}, \tag{6}$$

where $\Im m(\cdot)$ denotes the imaginary part (for later reference, $\Re e(\cdot)$ denotes the real part). The traction at the computational boundary ($x = 0$) is given by,

$$\mathbf{T}_x^{in}\Big|_{x=0} = -\left(\mathbf{G}_{xx}\frac{\partial}{\partial x} + ik_y\mathbf{G}_{xy}\right)\mathbf{u}|_{x=0}. \tag{7}$$

3.2. Reflection matrix

In the absence of sources in $x > 0$, an unbounded domain defined by $x \geqslant 0$ admits wavemodes of the form $\mathbf{u} = \mathbf{a}e^{ik_x x}$ where the wavenumber, wavemode pair $(k_x, \mathbf{a})$ is an eigenpair of the quadratic eigenvalue problem $\mathbf{\Lambda}^{in}\mathbf{a} = \mathbf{0}$ with k_x satisfying (5) i.e. it admits only outgoing modes. A finite layer obtained by truncating the unbounded domain at $x = L > 0$ admits both outgoing and incoming wavemodes. In the absence of sources in $0 < x \leqslant L$, the incoming modes can be seen as

reflections of the outgoing modes generated at the truncation boundary condition. The total wavefield in this case can be written as (see [26]),

$$\mathbf{u} = \left(\mathbf{X}\mathbf{P}(x) + \widetilde{\mathbf{X}}\widetilde{\mathbf{P}}(x-L)\mathbf{R}_T\mathbf{P}(L)\right)\Gamma, \tag{8}$$

where $\mathbf{X}$ denotes the matrix of all *outgoing* normalized eigenvectors, $\widetilde{\mathbf{X}}$ denotes the matrix of all *incoming* normalized eigenvectors and normalization implies $\|\mathbf{X}(\cdot,j)\| = 1,\ \left\|\widetilde{\mathbf{X}}(\cdot,j)\right\| = 1,\ \forall j \in (1,2)$. $\mathbf{P}(x) = diag\left(e^{ik_{x1}x}, e^{ik_{x2}x}\right)$ and $\widetilde{\mathbf{P}}(x) = diag\left(e^{i\widetilde{k_{x1}}x}, e^{i\widetilde{k_{x2}}x}\right)$ are the propagator matrices with $k_{x1},\ k_{x2}$ satisfying (5) and $\widetilde{k_{x1}},\ \widetilde{k_{x2}}$ satisfying (6). $\mathbf{R}_T$ here represents the reflection matrix associated with truncation at $x = L$. Any purely outgoing wave can be expressed as $\mathbf{X}\mathbf{P}(x)\Gamma$ while any purely incoming wave can be expressed as $\widetilde{\mathbf{X}}\widetilde{\mathbf{P}}(x)\widetilde{\Gamma}$, with $\Gamma,\ \widetilde{\Gamma}$ being the vectors of participation factors. Defining the computational reflection matrix as,

$$\mathbf{R}_C = \widetilde{\mathbf{P}}(-L)\mathbf{R}_T\mathbf{P}(L), \tag{9}$$

we can write $\mathbf{u}|_{x=0} = \left(\mathbf{X} + \widetilde{\mathbf{X}}\mathbf{R}_C\right)\Gamma$ with (9) being a measure of the reflections due to truncation.

3.3. PMDL properties

The PMDL formulation approximates the exterior right half-space stiffness with $n(<\infty)$ mid-point integrated linear finite element layers of lengths $L_1, \ldots, L_n$ followed by a homogeneous Dirichlet truncation boundary condition (see [17]). For the model problem in Fig. 2, the traction at the computational boundary of the exterior right half space is given by (7) and hence the (exact) stiffness of the right half space becomes

$$\mathbf{K}_{exact} = -\left(ik_x\mathbf{G}_{xx} + ik_y\mathbf{G}_{xy}\right). \tag{10}$$

k_x in (10) satisfies (5) because a right half-space can only support outgoing modes. The n-layer PMDL approximates (10) by $\mathbf{K}_n$, the stiffness of a n-layer mid-point integrated linear finite element mesh with a homogeneous Dirichlet truncation boundary on the right. The rationale behind this approximation can be found in the prequel to this paper [26]. We can determine the computational reflection matrix (9) by noting that the decay (or growth) in amplitude achieved as the wavemode progresses from left to the right of each layer is $(1 + ik_xL_j/2)/(1 - ik_xL_j/2)$ and that achieved as the mode progresses from right to the left of each layer is $\left(1 - i\widetilde{k_x}L_j/2\right)/\left(1 + i\widetilde{k_x}L_j/2\right)$ where k_x is the outgoing wavenumber (5) and $\widetilde{k_x}$ is the incoming (reflected) wavenumber (6) (see [17]). This leads us to the expressions,

$$\mathbf{P} = \begin{bmatrix} \prod_{j=1}^{n}\left(\frac{2i/L_j - k_{x1}}{2i/L_j + k_{x1}}\right) & 0 \\ 0 & \prod_{j=1}^{n}\left(\frac{2i/L_j - k_{x2}}{2i/L_j + k_{x2}}\right) \end{bmatrix}, \quad \widetilde{\mathbf{P}} = \begin{bmatrix} \prod_{j=1}^{n}\left(\frac{2i/L_j + \widetilde{k_{x1}}}{2i/L_j - \widetilde{k_{x1}}}\right) & 0 \\ 0 & \prod_{j=1}^{n}\left(\frac{2i/L_j + \widetilde{k_{x2}}}{2i/L_j - \widetilde{k_{x2}}}\right) \end{bmatrix}. \tag{11}$$

In (11), $k_{x1}\left(\widetilde{k_{x1}}\right)$ and $k_{x2}\left(\widetilde{k_{x2}}\right)$ are the outgoing (incoming) horizontal wavenumbers (see Fig. 3b). In cases where the distinction of pressure and shear waves can be clearly made, like in elliptic anisotropy, we can assume $k_{x1}\left(\widetilde{k_{x1}}\right)$ and $k_{x2}\left(\widetilde{k_{x2}}\right)$ to refer to pressure and shear wavemodes respectively. The expressions in (11) along with (9) give us the reflection matrix at the computational boundary $\mathbf{R}_C$. Of the three matrices $\mathbf{P},\ \widetilde{\mathbf{P}},\ \mathbf{R}_T$, the matrices $\mathbf{P},\ \widetilde{\mathbf{P}}$ depend on the PMDL parameters (the layer lengths) while $\mathbf{R}_T$ depends on the truncation boundary at the end of PMDL. Each element $\mathbf{R}_C(\xi,\eta)$ takes the form, from (11) and (9):

$$\mathbf{R}_C(\xi,\eta) = \widetilde{\mathbf{P}}(\xi,\xi)\mathbf{R}_T(\xi,\eta)\mathbf{P}(\eta,\eta) = \underbrace{\mathbf{R}_T(\xi,\eta)}_{truncationBC}\underbrace{\left(\prod_{j=1}^{n}\left(\frac{2i/L_j + \widetilde{k_{x\xi}}}{2i/L_j - \widetilde{k_{x\xi}}}\right)\left(\frac{2i/L_j - k_{x\eta}}{2i/L_j + k_{x\eta}}\right)\right)}_{PMDL\ \ contribution} \quad \forall \xi,\eta \in \{1,2\}. \tag{12}$$

We assume that $\mathbf{R}_T \neq \mathbf{0}$ and the elements of $\mathbf{R}_T$ are bounded independent of (k_x, k_y); this is typical e.g. the homogeneous Dirichlet boundary condition considered here satisfies these assumptions.

4. Accuracy

In order to facilitate later derivations, using the notation in Fig. 3b, we define,

$$R_j(\xi,\eta) = \left(\frac{\widetilde{\sigma_{x\xi}} + \sigma_{xj}^{ref}}{\widetilde{\sigma_{x\xi}} - \sigma_{xj}^{ref}}\right)\left(\frac{\sigma_{x\eta} - \sigma_{xj}^{ref}}{\sigma_{x\eta} + \sigma_{xj}^{ref}}\right) \quad \forall \xi,\eta \in \{1,2\}, \tag{13}$$

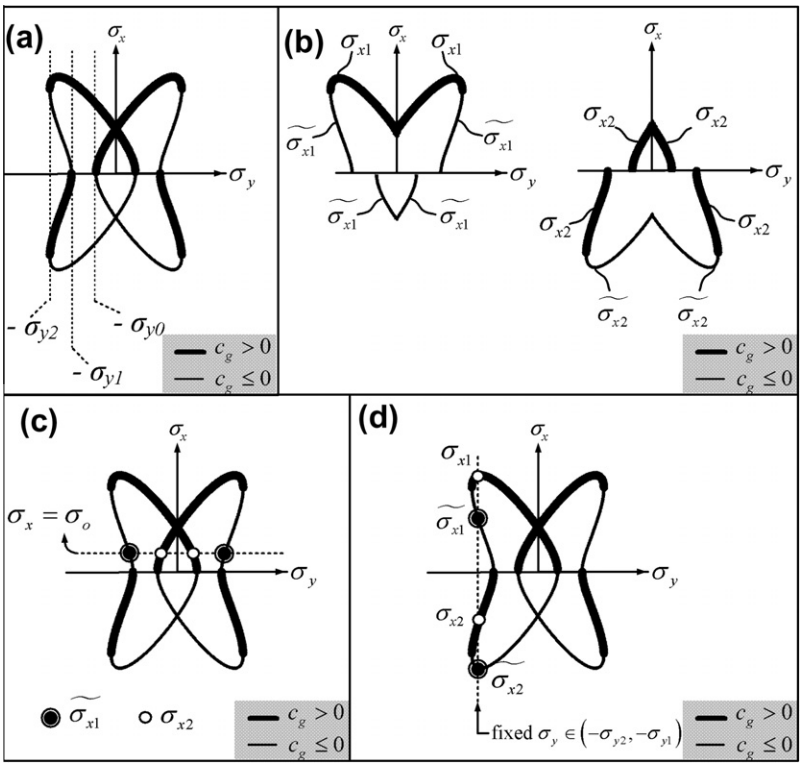

Fig. 3. (a) Demarcation of outgoing and incoming propagating slownesses using specific vertical slownesses $\sigma_{y0},\ \sigma_{y1},\ \sigma_{y2}$. (b) Notation for representing outgoing and incoming propagating horizontal slownesses ($\sigma_x \in \mathbb{R}$). $\sigma_{x1},\ \sigma_{x2}$ represent the horizontal slownesses for outgoing wavemodes and $\widetilde{\sigma_{x1}},\ \widetilde{\sigma_{x2}}$ represent the horizontal slownesses for incoming wavemodes. (c) Both outgoing and incoming wavemodes with the same horizontal slowness σ_o. (d) Various horizontal slownesses for a fixed vertical slowness $\sigma_y \in (-\sigma_{y2}, -\sigma_{y1})$.

where, $\sigma_{xj}^{ref} = 2i/\omega L_j$ is the jth PMDL parameter with L_j being the PMDL layer length and, $\sigma_{x1,2}$ and $\widetilde{\sigma_{x1,2}}$ being respectively the outgoing and incoming horizontal slownesses for the two in-plane wavemodes. Writing (12) using slownesses instead of wavenumbers and then using (13) results in,

$$\mathbf{R}_C(\xi,\eta) = \underbrace{\mathbf{R}_T(\xi,\eta)}_{\substack{\text{truncation}\\ \text{BC}}} \underbrace{\mathbf{R}_{PMDL}(\xi,\eta)}_{\text{PMDL contribution}} \quad \forall \xi,\eta \in \{1,2\}, \tag{14}$$

where,

$$\mathbf{R}_{PMDL}(\xi,\eta) = \left(\prod_{j=1}^{n} R_j(\xi,\eta)\right) \quad \text{for} \quad n-\text{layer PMDL}. \tag{15}$$

It can be clearly seen from Eqs. (13)–(15) that a choice of PMDL layer lengths of $L_j = 2i/\omega\sigma_{xj}^{ref}$ will make the n-layer PMDL exact for a choice of slownesses $\sigma_x = \sigma_{xj}^{ref}$. Hence σ_{xj}^{ref} are the interpolation points for the approximation of (10) by the n-layer PMDL stiffness ($\mathbf{K}_n$). $\sigma_{x1}^{ref}, \sigma_{x2}^{ref}, \ldots, \sigma_{xn}^{ref}$ are thus the parameters of PMDL, also known as its reference slownesses.

4.1. Accuracy criterion

An ABC is considered exact if $\mathbf{R}_C(\xi,\eta) = 0$ for all $\xi,\eta \in \{1,2\}$. Accuracy of an approximate ABC hence translates to making $\mathbf{R}_C(\xi,\eta)$ as small as possible. Typically the accuracy of ABCs is a function of the ABC parameters and the computational effort that can be reasonably expended. For an ABC to be considered accurate in any sense, it has to be convergent i.e., it should yield the exact solution in the limit of infinite computational effort. In other words, an ABC is termed accurate if its parameters can be chosen to yield $\mathbf{R}_C(\xi,\eta) \to 0$ with increasing computational effort.

Accuracy criterion: A n-layer PMDL is considered accurate if, by increasing the number of layers n, the magnitude of every element of its computational reflection matrix can be made arbitrarily small for every wavemode, i.e.,

$$\lim_{n\to\infty} |\mathbf{R}_C(\xi,\eta)| = 0 \quad \forall \xi,\eta \in \{1,2\} : \begin{array}{l}\text{Accuracy criterion for}\\ n-\text{layer PMDL}\end{array}. \tag{16}$$

To be precise (16) is a *convergence* criterion; the usage of the term *accuracy* instead of the term *convergence* is mainly for the sake of compatibility with existing ABC literature [47].

For a homogeneous Dirichlet truncation boundary condition, the elements of $\mathbf{R}_T$ are independent of the slownesses, finite and non-zero, and hence using (14), (16) reduces to,

$$\lim_{n\to\infty}|\mathbf{R}_{PMDL}(\xi,\eta)| = 0 \quad \forall \xi,\eta \in \{1,2\} : \frac{\text{Accuracy criterion for}}{n-\text{layer PMDL}}. \tag{17}$$

4.2. Accuracy criterion for layer groups

For later use we specify a more general accuracy criterion that is a modification of the criterion given in the previous section. To facilitate this, we define a $m \times n$-layer PMDL ($m \geqslant 1, n \geqslant 1$) as a PMDL with mn layers that is viewed as made up of n groups of m layers each. Note that a $m \times n$-layer PMDL is just a regular PMDL viewed differently. We now define the following modified accuracy criterion.

Accuracy criterion: A $m \times n$-layer PMDL is considered accurate if, by increasing the number of *groups (n)*, the magnitude of every element of its computational reflection matrix can be made arbitrarily small for every wavemode, i.e.,

$$\lim_{n\to\infty}|\mathbf{R}_{C}(\xi,\eta)| = 0 \quad \forall \xi,\eta \in \{1,2\} : \frac{\text{Accuracy criterion for}}{m\times n-\text{layer PMDL}}. \tag{18}$$

As before, (18) reduces to,

$$\lim_{n\to\infty}|\mathbf{R}_{PMDL}(\xi,\eta)| = 0 \quad \forall \xi,\eta \in \{1,2\} : \frac{\text{Accuracy criterion for}}{m\times n-\text{layer PMDL}}. \tag{19}$$

The only difference between (19) and (17) is the *way* in which we increase the total number of layers. For (19), we increase the number of *groups* with a fixed number of layers per group. To complete this distinction, we rewrite (15) in a grouped form as

$$\mathbf{R}_{PMDL}(\xi,\eta) = \prod_{p=1}^{n}\left(\prod_{s=1}^{m} R_{m\cdot p-(s-1)}(\xi,\eta)\right) \quad \text{for} \quad m\times n-\text{layer PMDL}. \tag{20}$$

Of course, (17) is just a special case of (19) with groups of 1 layer each, or in other words (17) is the accuracy criterion for a $1 \times n$ layer PMDL. We will hence use (20) for all later calculations. The utility of grouping will become evident in the next section.

4.3. Sufficient conditions for accuracy

A simple sufficient condition for accuracy of a $m \times n$-layer PMDL obtained by using (20) in (19) is

$$\left|\prod_{s=1}^{m} R_{m\cdot p-(s-1)}(\xi,\eta)\right| = \left|\prod_{s=1}^{m}\left(\frac{\widetilde{\sigma_{x\xi}} + \sigma^{ref}_{x(m\cdot p-(s-1))}}{\widetilde{\sigma_{x\xi}} - \sigma^{ref}_{x(m\cdot p-(s-1))}}\right)\left(\frac{\sigma_{x\eta} - \sigma^{ref}_{x(m\cdot p-(s-1))}}{\sigma_{x\eta} + \sigma^{ref}_{x(m\cdot p-(s-1))}}\right)\right| < 1, \quad \forall \xi,\eta \in \{1,2\},\ p = (1\ldots n). \tag{21}$$

Note that the advantage of the grouping in (21) is that we now have m parameters to choose, $\sigma^{ref}_{x(m\cdot p)}, \sigma^{ref}_{x(m\cdot p-1)}, \ldots, \sigma^{ref}_{x(m\cdot p-(m-1))}$, to ensure accuracy. Each layer need not satisfy $|R_j(\xi,\eta)| < 1$ by itself; only a group of every m layers together need to satisfy (21). Of course this is at the cost of efficiency and for a given total number of layers, satisfying $|R_j(\xi,\eta)| < 1$ for every layer will lead to faster convergence as compared to satisfying the inequality in (21).

It should be noted that there are multiple ways of grouping layers e.g. a PMDL with a total of 8 layers can be viewed as a $1\times 8,\ 2\times 4,\ 4\times 2$ or 8×1 layer PMDL with 1, 2, 4 and 8 parameters respectively to choose from to ensure (21). Therefore (21) defines a *sequence* of successively less conservative sufficient conditions with increasing m. We can simplify (21) by dropping the index p and deriving conditions on the m arbitrary parameters $\sigma^{ref}_{x1}, \sigma^{ref}_{x2}, \ldots, \sigma^{ref}_{xm}$ to satisfy (21). Hence a sufficient condition for accuracy of a $m \times n$-layer PMDL is

$$\left|\prod_{s=1}^{m} R_{s}(\xi,\eta)\right| = \left|\prod_{s=1}^{m}\left(\frac{\widetilde{\sigma_{x\xi}} + \sigma^{ref}_{xs}}{\widetilde{\sigma_{x\xi}} - \sigma^{ref}_{xs}}\right)\left(\frac{\sigma_{x\eta} - \sigma^{ref}_{xs}}{\sigma_{x\eta} + \sigma^{ref}_{xs}}\right)\right| < 1 \quad \forall \xi,\eta \in \{1,2\}. \tag{22}$$

To simplify later notation we define:

$$r_m\left(\sigma_x, \sigma^{ref}_{x1}, \ldots, \sigma^{ref}_{xm}\right) = \prod_{s=1}^{m}\left(\frac{\sigma_x - \sigma^{ref}_{xs}}{\sigma_x + \sigma^{ref}_{xs}}\right). \tag{23}$$

Using (23) in (22) we get

$$\left|\prod_{s=1}^{m} R_s(\xi,\eta)\right| = \left|r_m\left(\sigma_{x\eta}, \sigma_{x1}^{ref}, \ldots, \sigma_{xm}^{ref}\right)\right| \left|r_m\left(\widetilde{\sigma_{x\xi}}, \sigma_{x1}^{ref}, \ldots, \sigma_{xm}^{ref}\right)\right|^{-1} < 1 \quad \forall \xi,\eta \in \{1,2\}. \tag{24}$$

The form in (24) uses the notation $r_m\left(\sigma_x, \sigma_{x1}^{ref}, \ldots, \sigma_{xm}^{ref}\right)$ to underscore the dependence of r_m on the horizontal wavenumber and the m parameters of PMDL; r_m in this case is termed *σ_y-independent* because there is no explicit dependence on σ_y. E.g. in Fig. 3c, $r_m\left(\sigma_o, \sigma_{x1}^{ref}, \ldots, \sigma_{xm}^{ref}\right)$ is a constant at all the four points shown for a given set of parameters $\left(\sigma_{x1}^{ref}, \ldots, \sigma_{xm}^{ref}\right)$.

4.4. Necessary conditions for accuracy

The expression in (24) provides, as mentioned before, a sequence of progressively *less* conservative sufficient conditions. A simple necessary condition then can be stated as:

There exists an $m < \infty$ for which (24) is satisfied for all propagating wavemodes. (25)

If (24) is not satisfied for *any* m, that implies that there exists no layer grouping that provides accuracy. As $m \to \infty$ if every $\left|\prod_{s=1}^{m} R_{m\cdot j-(s-1)}(\xi,\eta)\right| \geqslant 1$, then we can see from (20) that (19) can no longer be satisfied, indicating that it is not possible for the ABC to be accurate..

Another necessary condition is,

$$\sigma_{xj}^{ref} \neq \widetilde{\sigma_{x\xi}} \quad \forall \xi = \{1,2\}. \tag{26}$$

The necessity of (26) is fairly obvious. For if $\sigma_{xj}^{ref} = \widetilde{\sigma_{x\xi}} \neq 0$ for a pair (ξ, j), $|R_j(\xi,\eta)| = \infty$ since $\sigma_{x\eta} \neq \widetilde{\sigma_{x\xi}} \quad \forall \xi,\eta = \{1,2\}$ and (17) cannot be achieved. If $\sigma_{xj}^{ref} = \widetilde{\sigma_{x\xi}} = 0$, this implies an infinite layer length L_j (since $\sigma_{xj}^{ref} = 2i/\omega L_j$) which is not implementable. Since σ_{xj}^{ref} represent the points of interpolation, (26) simply implies that we cannot interpolate the wrong branch (6) of the slowness diagram. In a sense an infinite element of the reflection matrix implies that the ABC allows purely incoming wavemodes in the absence of outgoing modes. This mimics spurious input of energy from the exterior leading to inaccuracies and instabilities.

5. Design and implementation of an accurate PMDL

In this section, we first show that irrespective of how large m is, it is impossible to satisfy (24) for all the propagating wavemodes of untilted non-elliptic anisotropic elasticity with a traditional PMDL having *σ_y-independent* parameters $\sigma_{xj}^{ref} \in \mathbb{C}$. We then determine the conditions on the real-valued, *σ_y-dependent* parameters $\sigma_{xj}^{ref}(\sigma_y) \in \mathbb{R}$ required to satisfy (24) with the smallest m. These conditions are sufficient to absorb all outgoing propagating wavemodes but are not implementable. Their implementation is eventually facilitated by noting that the choice of *σ_y-dependent* parameters $\sigma_{xj}^{ref}(\sigma_y)$ can be viewed as an unconventional stretching of the finite element PMDL mesh.

5.1. Inadequacy of wavenumber-independent parameters

In standard PMDL, the parameters σ_{xj}^{ref} are independent of the vertical wavenumber σ_y. In this sub-section, we simply show that for *any* given set of *σ_y-independent* parameters, there exists a propagating wavemode ($\sigma_x \in \mathbb{R}$) such that (24) cannot be satisfied for any m. According to (25), this proves that it is impossible to design an accurate PMDL with *σ_y-independent* σ_{xj}^{ref}.

Using (24), and the fact that the slowness diagram is symmetric about the σ_y axis (see Fig. 3a,b), we make the following simple observations:

$$\begin{aligned} &\sigma_{x1} = -\widetilde{\sigma_{x2}}, \\ &\sigma_{x2} = -\widetilde{\sigma_{x1}}, \\ &\left|r_m\left(\sigma_x \sigma_{x1}^{ref}, \ldots, \sigma_{xm}^{ref}\right)\right| = \left|r_m\left(-\sigma_x,\ \sigma_{x1}^{ref}, \ldots, \sigma_{xm}^{ref}\right)\right|^{-1}. \end{aligned} \tag{27}$$

Consider an arbitrary fixed $\sigma_x = \sigma_o > 0$ such that there exist both outgoing and incoming wavemodes with the horizontal wavenumber σ_o i.e., using our standard notation we choose a $\sigma_o > 0$ such that there exists $\widetilde{\sigma_{x1}} = \sigma_o,\ \sigma_{x2} = \sigma_o$ as shown in Fig. 3c. Also choose m arbitrary complex-valued PMDL parameters $\sigma_{x1}^{ref}, \sigma_{x2}^{ref}, \ldots, \sigma_{xm}^{ref}$. For the given σ_o, the choice of parameters could be such that $\left|r_m\left(\sigma_o, \sigma_{x1}^{ref}, \ldots, \sigma_{xm}^{ref}\right)\right| < 1$, $\left|r_m\left(\sigma_o, \sigma_{x1}^{ref}, \ldots, \sigma_{xm}^{ref}\right)\right| > 1$ or $\left|r_m\left(\sigma_o, \sigma_{x1}^{ref}, \ldots, \sigma_{xm}^{ref}\right)\right| = 1$. Consider the three separate cases:

Case 1: $|r_m(\sigma_o,\cdot)| < 1$. Since there exists an incoming wavemode $\widetilde{\sigma_{x1}} = \sigma_o$ (see Fig. 3c), we have $\left|r_m(\widetilde{\sigma_{x1}},\cdot)\right| < 1$. Using (27) and $\sigma_{x2} = -\widetilde{\sigma_{x1}}$, we get $\left|r_m(\widetilde{\sigma_{x1}},\cdot)\right| = \left|r_m(-\widetilde{\sigma_{x1}},\cdot)\right|^{-1} = |r_m(\sigma_{x2},\cdot)|^{-1}$. Hence $|r_m(\sigma_{x2},\cdot)|^{-1} < 1$ or equivalently $|r_m(\sigma_{x2},\cdot)|\left|r_m(\widetilde{\sigma_{x1}},\cdot)\right|^{-1} > 1$. This implies $\left|\prod_{s=1}^{m} R_s(1,2)\right| > 1$, thus violating (24).

Case2: $|r_m(\sigma_o,\cdot)|>1$. Since there exists an outgoing wavemode $\sigma_{x2}=\sigma_o$ (see Fig. 3c), we have $|r_m(\sigma_{x2},\cdot)|>1$. Similar to the previous paragraph, we get $\left|r_m\left(\widetilde{\sigma_{x1}},\cdot\right)\right|=|r_m(\sigma_{x2},\cdot)|^{-1}$ and hence $|r_m(\sigma_{x2},\cdot)|\left|r_m\left(\widetilde{\sigma_{x1}},\cdot\right)\right|^{-1}>1$. This implies $\left|\prod_{s=1}^{m}R_s(1,2)\right|>1$, which violates (24).

Case 3: $|r_m(\sigma_o,\cdot)|=1$. By the same arguments as above, there exists $\left|\prod_{s=1}^{m}R_s(1,2)\right|=1$ that violates (24).

Since both m and the parameters of PMDL were completely arbitrary, the above analysis shows that (24) cannot be satisfied with any number of σ_y-*independent* parameters.

A more intuitive reason for the inadequacy of σ_y-*independent* σ_{xj}^{ref} can be obtained by noting the necessary condition for accuracy (26). According to (26), the parameters of PMDL σ_{xj}^{ref} should not interpolate the incoming branch of the slowness diagram i.e. it should not cut the *thin* lines in Fig. 5d. We cannot achieve this by σ_y -*independent* σ_{xj}^{ref}; such σ_{xj}^{ref} are represented as horizontal lines on the slowness figure and they always cut one of the thin lines when they are within the bounds of the slowness diagram (not too far above or below). Only inclined lines as shown in Fig. 5d will escape cutting the thin lines and σ_{xj}^{ref} represented by such inclined lines are σ_y -*dependent*. Of course, the above argument no longer holds when the σ_y -*independent* σ_{xj}^{ref} form horizontal lines far above the top or far below the bottom of the slowness diagram and to exclude those cases precisely we need the mathematical analysis provided above.

5.2. Wavenumber-dependent parameters: requirements

The previous subsection revealed the fact that it is the presence of both outgoing and incoming wavemodes with identical horizontal wavenumbers σ_o that makes it impossible to satisfy (24). In fact, the deeper reason behind it is that the PMDL parameters are independent of σ_y. For, even though both σ_{x2} and $\widetilde{\sigma_{x1}}$ are equal to σ_o, they occur at different σ_y as evident from Fig. 3c and this may be used to our advantage to satisfy (24).

For propagating wavemodes ($\sigma_x\in\mathbb{R}$), it can be easily shown that we cannot satisfy (24) with a $1\times n$ layer PMDL even with σ_y-*dependent* parameters. Consider for example σ_{x1}^{ref} (note that $m=1$ for a $1\times n$ layer PMDL) to be an arbitrary complex function of σ_y i.e. $\sigma_{x1}^{ref}(\sigma_y)\in\mathbb{C}$. Consider now a fixed $\sigma_y\in(-\sigma_{y2},-\sigma_{y1})$ as shown in Fig. 3d. At this fixed σ_y we have two outward propagating wavemodes $\sigma_{x1}>0$, $\sigma_{x2}<0$ and two inward propagating modes $\widetilde{\sigma_{x1}}>0$, $\widetilde{\sigma_{x2}}<0$ as shown in Fig. 3d. Also at this fixed σ_y, $\sigma_{x1}^{ref}(\sigma_y)$ is a constant complex number with either $\Re e\left(\sigma_{x1}^{ref}(\sigma_y)\right)>0$, or $\Re e\left(\sigma_{x1}^{ref}(\sigma_y)\right)<0$, or $\Re e\left(\sigma_{x1}^{ref}(\sigma_y)\right)=0$. Consider the three separate cases:

Case 1: $\Re e\left(\sigma_{x1}^{ref}(\sigma_y)\right)>0$. Checking (13) with $\widetilde{\sigma_{x1}}>0$ and $\sigma_{x2}<0$, we can easily conclude that $|R_j(1,2)|>1$ i.e. (24) is not satisfied.

Case 2: $\Re e\left(\sigma_{x1}^{ref}(\sigma_y)\right)<0$. Checking (13) with $\widetilde{\sigma_{x2}}<0$ and $\sigma_{x1}>0$, we can conclude that $|R_j(2,1)|>1$, i.e., (24) is again not satisfied.

Case 3: $\Re e\left(\sigma_{xj}^{ref}(\sigma_y)\right)=0$. Checking (13) we see that the numerator and denominator will be complex conjugates with $|R_j(\cdot,\cdot)|=1$, i.e., (24) is not satisfied.

Given that the above analysis proves that a $1\times n$ layer PMDL will not work, we now examine whether a two layer grouping, i.e., a $2\times n$ layer PMDL, can satisfy (24) and guarantee accuracy, first with $\sigma_{xj}^{ref}(\sigma_y)\in\mathbb{R}$. We resort to the earlier notation of σ_{x1}^{ref}, σ_{x2}^{ref} with the understanding that henceforth, σ_{xj}^{ref} will be a function of σ_y. Moreover, now $r_2(\cdot)$ is also a function of σ_y, but we will again drop the σ_y. For a $2\times n$ layer PMDL, (24) can simply be satisfied by ensuring

$$\left|r_2\left(\sigma_{x\eta},\sigma_{x1}^{ref},\sigma_{x2}^{ref}\right)\right|<1,\quad \left|r_2\left(\widetilde{\sigma_{x\xi}},\sigma_{x1}^{ref},\sigma_{x2}^{ref}\right)\right|\geqslant 1\quad\forall\xi,\eta\in\{1,2\}. \tag{28}$$

The inequalities in (28) essentially imply that the choice of the PMDL parameters σ_{x1}^{ref}, σ_{x2}^{ref} should be such that the rational function $r_2(\sigma_x,\cdot)$ should have a magnitude less than 1 for outgoing σ_x and a magnitude greater than or equal to 1 for incoming σ_x. If, for a given set of PMDL parameters σ_{x1}^{ref}, σ_{x2}^{ref}, we can determine the regions in $\sigma_x\in(-\infty,\infty)$ for which $\left|r_2\left(\sigma_x,\sigma_{x1}^{ref},\sigma_{x2}^{ref}\right)\right|<1$, we might be able to ensure all outgoing σ_x to fall within these regions and all incoming σ_x to fall outside these regions thus satisfying (28).

We reassert that we are considering real-valued PMDL parameters and propagating waves, i.e., σ_x, σ_{x1}^{ref}, $\sigma_{x2}^{ref}\in\mathbb{R}$. Without loss of generality we assume $\left|\sigma_{x1}^{ref}\right|>\left|\sigma_{x2}^{ref}\right|$. Expanding $r_2(\sigma_x,\cdot)$ using (23) and noting that all variables are real-valued, we get the following:

$$\begin{aligned}|r_2(\sigma_x,\cdot)|<1 &\iff \left|\left(\sigma_x^2+\sigma_{x1}^{ref}\sigma_{x2}^{ref}\right)-\sigma_x\left(\sigma_{x1}^{ref}+\sigma_{x2}^{ref}\right)\right|<\left|\left(\sigma_x^2+\sigma_{x1}^{ref}\sigma_{x2}^{ref}\right)+\sigma_x\left(\sigma_{x1}^{ref}+\sigma_{x2}^{ref}\right)\right|\\ &\iff \left(\sigma_x^2+\sigma_{x1}^{ref}\sigma_{x2}^{ref}\right)\sigma_x\left(\sigma_{x1}^{ref}+\sigma_{x2}^{ref}\right)>0.\end{aligned} \tag{29}$$

Depending on the values of the parameters σ_{x1}^{ref} and σ_{x2}^{ref}, Eq. (29) is satisfied on different regions of σ_x. These regions are enumerated below for later convenience.

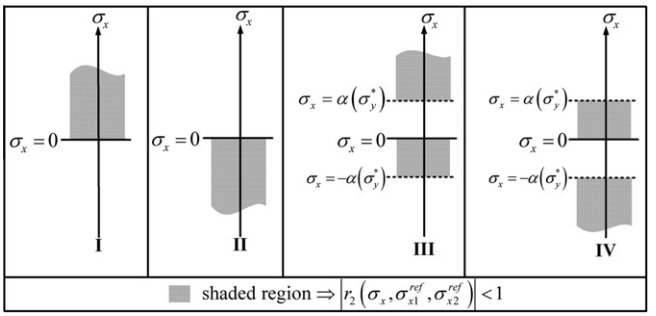

Fig. 4. Regions with $\left|r_2\left(\sigma_x, \sigma_{x1}^{ref}, \sigma_{x2}^{ref}\right)\right| < 1$ for a 2-layer grouping of PMDL for a fixed $\sigma_y = \sigma_y^*$.

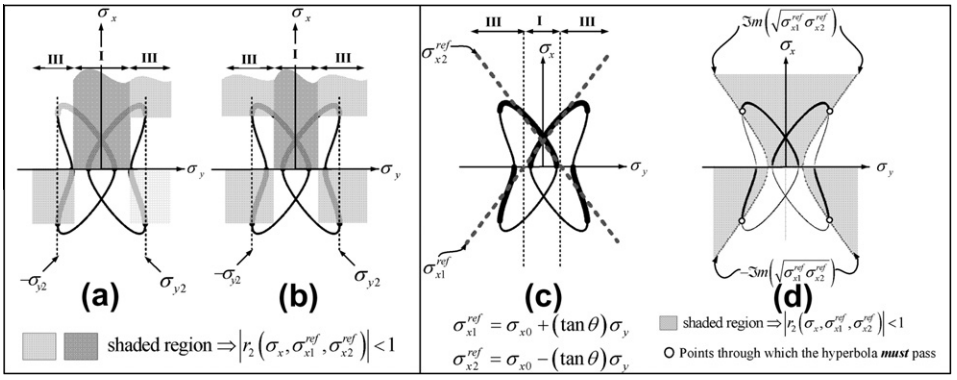

Fig. 5. (a), (b) Valid choices that ensure *only* the outgoing wavemodes (thick lines) fall in the shaded region and consequently the incoming wavemodes (thin lines) fall outside the shaded region. (c) The two PMDL parameters that are linearly dependent on vertical slownesses σ_y for a 2-layer grouping. (d) Shaded regions with $|r_2(\sigma_x, \cdot)| < 1$ for the parameters that are linearly dependent on σ_y. Note that all the outgoing wavemodes (thick lines) fall in the shaded region while all the incoming wavemodes (thin lines) fall outside the shaded region.

$$
\begin{aligned}
&\sigma_{x1}^{ref} > 0,\ \sigma_{x2}^{ref} > 0: \quad |r_2(\sigma_x, \cdot)| < 1 \quad \forall \sigma_x \in (0, \infty) \quad \mathbf{I}\\
&\sigma_{x1}^{ref} < 0,\ \sigma_{x2}^{ref} < 0: \quad |r_2(\sigma_x, \cdot)| < 1 \quad \forall \sigma_x \in (-\infty, 0) \quad \mathbf{II}\\
&\sigma_{x1}^{ref} > 0,\ \sigma_{x2}^{ref} < 0: \quad |r_2(\sigma_x, \cdot)| < 1 \quad \forall \sigma_x \in (-\alpha(\sigma_y), 0) \cup (\alpha(\sigma_y), +\infty) \quad \mathbf{III}\\
&\sigma_{x1}^{ref} < 0,\ \sigma_{x2}^{ref} > 0: \quad |r_2(\sigma_x, \cdot)| < 1 \quad \forall \sigma_x \in (-\infty, -\alpha(\sigma_y)) \cup (0, \alpha(\sigma_y)) \quad \mathbf{IV}.
\end{aligned}
\tag{30}
$$

In the above $\alpha(\sigma_y) = \left|\sigma_{x1}^{ref}\sigma_{x2}^{ref}\right|^{1/2}$. Implications of (30) are shown in Fig. 4 for a fixed $\sigma_y = \sigma_y^*$. Comparing Fig. 4 with the slowness diagram that we wish to capture (thick line in Fig. 3a), we can easily see that (28) can be satisfied if $\sigma_{x\eta}$ falls *within* the four regions ($\mathbf{I}, \ldots, \mathbf{IV}$) specified by (30) and $\widetilde{\sigma_{x\xi}}$ falls *outside* these regions. Hence for example, one valid choice of σ_{x1}^{ref}, σ_{x2}^{ref} could be such that for $\sigma_y \in (-\sigma_{y2}, -\sigma_{y1}) \cup (\sigma_{y1}, \sigma_{y2})$, σ_x falls in region **III** and for $\sigma_y \in (-\sigma_{y1}, \sigma_{y1})$, σ_x falls in region **I** (see Fig. 5a) i.e. $\sigma_{x1}^{ref} > 0$, $\sigma_{x2}^{ref} < 0$ for $\sigma_y \in (-\sigma_{y2}, -\sigma_{y1}) \cup (\sigma_{y1}, \sigma_{y2})$ and $\sigma_{x1}^{ref} > 0$, $\sigma_{x2}^{ref} > 0$ for $\sigma_y \in (-\sigma_{y1}, \sigma_{y1})$.

The above analysis shows that the σ_y-*dependent* parameters $\sigma_{x1}^{ref}, \sigma_{x2}^{ref}$ should at least change signs over different intervals of σ_y. Linear dependence on σ_y will provide a simple choice of such parameters and we can assume $\sigma_{x1}^{ref} = \sigma_{x0} + (\tan\theta)\sigma_y$, $\sigma_{x2}^{ref} = \sigma_{x0} - (\tan\theta)\sigma_y$ (Fig. 5c). The usage of $\pm\tan\theta$ is suggested by the symmetry of the slowness diagram with respect to σ_y. Such a choice leads to the bounds $\pm\alpha(\sigma_y)$ in (30) being defined by a hyperbola shown in Fig. 5d where the shaded regions have $|r_2(\sigma_x, \cdot)| < 1$. Note that $\pm\alpha(\sigma_y)$ forms the bound only in region **III**; region **I** has a lower bound of zero according to (30).

Knowing that **(a)** the positioning of the hyperbola should be such that the outgoing wavemodes $\sigma_{x\eta}$ fall within the regions specified by (30) and the incoming wavemodes $\widetilde{\sigma_{x\xi}}$ fall outside these regions and **(b)** the outgoing and incoming slownesses are identical at $\sigma_y = \pm\sigma_{y2}$, $\pm\sigma_{y1}$ and $\pm\sigma_{y0}$, we can conclude that *the hyperbola has to pass through the slowness at points* $\pm\sigma_{y2}$ *and should cross the* σ_y *axis in the intervals* $[-\sigma_{y1}, -\sigma_{y0}]$ *and* $[\sigma_{y0}, \sigma_{y1}]$. Since the hyperbola forms a bound only for region **III** and as $\sigma_{x1}^{ref}\sigma_{x2}^{ref} < 0$ there (see (30) and Fig. 5(c)), the hyperbola can be defined by $\pm\alpha(\sigma_y) = \pm\left(-\sigma_{x1}^{ref}\sigma_{x2}^{ref}\right)^{1/2} = \pm\left((\tan^2\theta)\sigma_y^2 - \sigma_{x0}^2\right)^{1/2}$ in region **III**. Moreover, since the bound for region **I** is zero, we can define the hyperbola over *both*

regions (**I** and **III**) simply as $\pm\Im m\left(\sigma_{x1}^{ref}\sigma_{x2}^{ref}\right)^{1/2}$; note that $\sigma_{x1}^{ref}\sigma_{x2}^{ref}>0$ in region **I** implies $\pm\Im m\left(\sigma_{x1}^{ref}\sigma_{x2}^{ref}\right)^{1/2}=0$ and $\sigma_{x1}^{ref}\sigma_{x2}^{ref}<0$ in region **III** implies $\pm\Im m\left(\sigma_{x1}^{ref}\sigma_{x2}^{ref}\right)^{1/2}=\pm\left(-\sigma_{x1}^{ref}\sigma_{x2}^{ref}\right)^{1/2}$. This is shown in Fig. 5d. A simple procedure can now be stated to obtain σ_{xo} and θ for the 2-layer grouping:

$$\begin{aligned}&(\mathbf{i})\ \text{Choose } \sigma_y^*\in\left[\sigma_{y0},\sigma_{y1}\right],\\ &(\mathbf{ii})\ \text{Determine } \sigma_{xo}=\frac{\sigma_{x1}|_{\sigma_y=\pm\sigma_{y2}}}{\left(\left(\frac{\sigma_{y2}}{\sigma_y^*}\right)^2-1\right)^{1/2}},\\ &(\mathbf{iii})\ \text{Get } \theta=\tan^{-1}\left(\frac{\sigma_{x0}}{\sigma_y^*}\right).\end{aligned}\tag{31}$$

Step **(i)** in (31) chooses an arbitrary σ_y^*, the apex of the hyperbola, i.e. $\alpha\left(\sigma_y^*\right)=0$, which implied $\tan\theta=\sigma_{xo}/\sigma_y^*$. Substituting this into the requirement $\alpha(\pm\sigma_{y2})=\sigma_x|_{\sigma_y=\pm\sigma_{y2}}$ we get **(ii)**. Of course, for our derivations to hold we should get $\sigma_{xo}\in\mathbb{R}$ and $\theta\in\mathbb{R}$, which is clearly seen graphically in Fig. 5d.

5.3. Wavenumber-dependent parameters: implementation

The previous subsection shows that it is theoretically possible to satisfy (19) with a $2\times n$ layer PMDL, provided we have σ_y-*dependent* σ_{xj}^{ref} of the form $\sigma_{xj}^{ref}=\sigma_{xo}\pm(\tan\theta)\sigma_y$. We will now specify a way to implement such a PMDL. Specifically, we show that an unconventional stretching of the PMDL mesh will be equivalent to providing $\sigma_{xj}^{ref}=\sigma_{xo}\pm(\tan\theta)\sigma_y$.

We consider a simple coordinate stretching of the form $x'=x/\cos\theta$ and $y'=y-x\tan\theta$ on (1) and Fourier transform it in y' to get the reduced wave equation of a transformed exterior,

$$\left(\mathbf{G}'_{xx}\frac{\partial^2}{\partial x'^2}+ik_y\left(\mathbf{G}'_{xy}+\mathbf{G}'^T_{xy}\right)\frac{\partial}{\partial x'}-\left(k_y^2\mathbf{G}'_{yy}-\omega^2\mathbf{I}\right)\right)\mathbf{u}'=\mathbf{0},\tag{32}$$

where the vertical wavenumber k_y remains the same as in (1) because $\partial/\partial y=\partial/\partial y'$ and the coefficient matrices are,

$$\begin{aligned}\mathbf{G}'_{xx}&=\frac{\mathbf{G}_{xx}}{\cos^2\theta},\\ \mathbf{G}'_{yy}&=\mathbf{G}_{xx}\tan^2\theta+\mathbf{G}_{yy}-\left(\mathbf{G}_{xy}+\mathbf{G}_{xy}^T\right)\tan\theta,\\ \mathbf{G}'_{xy}&=\frac{-\mathbf{G}_{xx}\tan\theta+\mathbf{G}_{xy}}{\cos\theta}.\end{aligned}\tag{33}$$

Such a transformed exterior is still 'perfectly matched' to the untransformed interior (see Appendix). The coordinate transformation is equivalent to stretching the exterior as shown in Fig. 6 and the stretched exterior can be approximated by stretched PMDL layers as shown in the same figure. The properties of these layers remain the same as in Section 3.3 with the transformed variables $\mathbf{G}'_{xx}$, $\mathbf{G}'_{yy}$, $\mathbf{G}'_{xy}$, $k_{x'}$, L'_j substituted for their original counterparts and L'_j being the PMDL layer length along x' (see Fig. 6b). The elements of $\mathbf{P}$, $\tilde{\mathbf{P}}$ in (11) and consequently the expression in (13) change accordingly to result in,

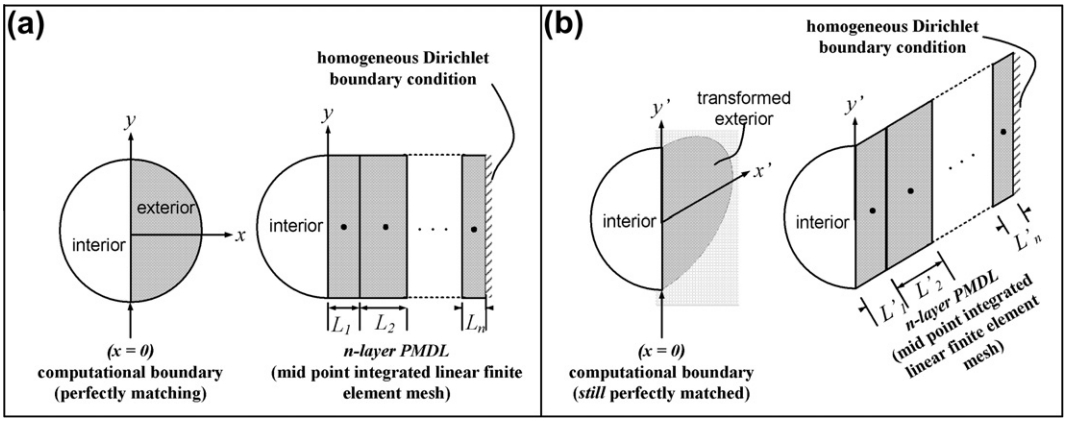

Fig. 6. Untransformed (a) and transformed (b) exterior with corresponding n-layer PMDL mesh.

$$R'_j(\xi,\eta)=\left(\frac{\widetilde{\sigma'_{x\xi}}+\sigma'^{(ref)}_{xj}}{\widetilde{\sigma'_{x\xi}}-\sigma'^{(ref)}_{xj}}\right)\left(\frac{\sigma'_{x\eta}-\sigma'^{(ref)}_{xj}}{\sigma'_{x\eta}+\sigma'^{(ref)}_{xj}}\right). \tag{34}$$

Using $k_{x'}=k_x\cos\theta+k_y\sin\theta$ and $\sigma'^{(ref)}_{xj}=\sigma^{ref}_{xj}\cos\theta$ (since $L'_j=L_j/\cos\theta$) in (34) we get,

$$R'_j(\xi,\eta)=\left(\frac{\widetilde{\sigma_{x\xi}}+\left(\sigma_y\tan\theta+\sigma^{ref}_{xj}\right)}{\widetilde{\sigma_{x\xi}}+\left(\sigma_y\tan\theta-\sigma^{ref}_{xj}\right)}\right)\left(\frac{\sigma_{x\eta}+\left(\sigma_y\tan\theta-\sigma^{ref}_{xj}\right)}{\sigma_{x\eta}+\left(\sigma_y\tan\theta+\sigma^{ref}_{xj}\right)}\right). \tag{35}$$

Note that (35) *cannot* be written in a form similar to (13) i.e. the above transformation of coordinates is *not* equivalent to (13) with σ_y-*dependent* σ^{ref}_{xj}. Or in other words a coordinate transformation $\sigma'_x=\sigma_x\cos\theta+\sigma_y\sin\theta$ is *not* equivalent to an identical transformation on the PMDL parameters, $\sigma'^{(ref)}_{xj}\neq\sigma^{ref}_x\cos\theta+\sigma_y\sin\theta$.

However, we note that we wish to eventually get $\sigma^{ref}_{xj}=\sigma_{x0}\pm(\tan\theta)\sigma_y$ i.e. with both $+\theta$ and $-\theta$. Hence, we look into a *group* of two PMDL layers, one designed for a transformed exterior similar to the one above with $(x,y)\xrightarrow{+\theta}(x',y')$ and the other designed for $(x,y)\xrightarrow{-\theta}(x'',y'')$. The previous arguments of perfect matching, being unaffected by coordinate transformations, still hold and the 2-layer condition of (22) transforms to,

$$R'_1(\xi,\eta)R''_2(\xi,\eta)=\left(\frac{\widetilde{\sigma'_{x\xi}}+\sigma'^{(ref)}_{x1}}{\widetilde{\sigma'_{x\xi}}-\sigma'^{(ref)}_{x1}}\right)\left(\frac{\sigma'_{x\eta}-\sigma'^{(ref)}_{x1}}{\sigma'_{x\eta}+\sigma'^{(ref)}_{x1}}\right)\left(\frac{\widetilde{\sigma''_{x\xi}}+\sigma''^{(ref)}_{x2}}{\widetilde{\sigma''_{x\xi}}-\sigma''^{(ref)}_{x2}}\right)\left(\frac{\sigma''_{x\eta}-\sigma''^{(ref)}_{x2}}{\sigma''_{x\eta}+\sigma''^{(ref)}_{x2}}\right). \tag{36}$$

Using $k_{x'}=k_x\cos\theta+k_y\sin\theta$, $k_{x''}=k_x\cos\theta-k_y\sin\theta$, $\sigma'^{(ref)}_{x1}=\sigma^{(ref)}_{x1}\cos\theta$ and $\sigma''^{(ref)}_{x2}=\sigma^{ref}_{x2}\cos\theta$ (since $L''_2=L_2/\cos\theta$ and $L'_1=L_1/\cos\theta$) in (36) we get,

$$\begin{aligned}R'_1(\xi,\eta)R''_2(\xi,\eta)=&\left(\frac{\widetilde{\sigma_{x\xi}}+\left(\sigma_y\tan\theta+\sigma^{ref}_{x1}\right)}{\widetilde{\sigma_{x\xi}}+\left(\sigma_y\tan\theta-\sigma^{ref}_{x1}\right)}\right)\left(\frac{\sigma_{x\eta}+\left(\sigma_y\tan\theta-\sigma^{ref}_{x1}\right)}{\sigma_{x\eta}+\left(\sigma_y\tan\theta+\sigma^{ref}_{x1}\right)}\right)\\&\times\left(\frac{\widetilde{\sigma_{x\xi}}+\left(-\sigma_y\tan\theta+\sigma^{ref}_{x2}\right)}{\widetilde{\sigma_{x\xi}}+\left(-\sigma_y\tan\theta-\sigma^{ref}_{x2}\right)}\right)\left(\frac{\sigma_{x\eta}+\left(-\sigma_y\tan\theta-\sigma^{ref}_{x2}\right)}{\sigma_{x\eta}+\left(-\sigma_y\tan\theta+\sigma^{ref}_{x2}\right)}\right).\end{aligned} \tag{37}$$

Rearranging (37) by shuffling the numerators and denominators, we can write,

$$\begin{aligned}R'_1(\xi,\eta)R''_2(\xi,\eta)=&\left(\frac{\widetilde{\sigma_{x\xi}}+\left(\sigma_y\tan\theta+\sigma^{ref}_{x1}\right)}{\widetilde{\sigma_{x\xi}}+\left(-\sigma_y\tan\theta-\sigma^{ref}_{x2}\right)}\right)\left(\frac{\sigma_{x\eta}+\left(-\sigma_y\tan\theta-\sigma^{ref}_{x2}\right)}{\sigma_{x\eta}+\left(\sigma_y\tan\theta+\sigma^{ref}_{x1}\right)}\right)\\&\times\left(\frac{\widetilde{\sigma_{x\xi}}+\left(-\sigma_y\tan\theta+\sigma^{ref}_{x2}\right)}{\widetilde{\sigma_{x\xi}}+\left(\sigma_y\tan\theta-\sigma^{ref}_{x1}\right)}\right)\left(\frac{\sigma_{x\eta}+\left(\sigma_y\tan\theta-\sigma^{ref}_{x1}\right)}{\sigma_{x\eta}+\left(-\sigma_y\tan\theta+\sigma^{ref}_{x2}\right)}\right),\end{aligned} \tag{38}$$

which, with the assumption $L_1=L_2$ (i.e. $\sigma^{ref}_{x1}=\sigma^{ref}_{x2}$), can be written as,

$$R'_1(\xi,\eta)R''_2(\xi,\eta)=\left(\frac{\widetilde{\sigma_{x\xi}}+{}_{+\theta}\sigma^{ref}_{x1}}{\widetilde{\sigma_{x\xi}}-{}_{+\theta}\sigma^{ref}_{x1}}\right)\left(\frac{\sigma_{x\eta}-{}_{+\theta}\sigma^{ref}_{x1}}{\sigma_{x\eta}+{}_{+\theta}\sigma^{ref}_{x1}}\right)\times\left(\frac{\widetilde{\sigma_{x\xi}}+{}_{-\theta}\sigma^{ref}_{x1}}{\widetilde{\sigma_{x\xi}}-{}_{-\theta}\sigma^{ref}_{x1}}\right)\left(\frac{\sigma_{x\eta}-{}_{-\theta}\sigma^{ref}_{x1}}{\sigma_{x\eta}+{}_{-\theta}\sigma^{ref}_{x1}}\right), \tag{39}$$

where,

$$\begin{aligned}{}_{+\theta}\sigma^{ref}_{x1}&=\sigma^{ref}_{x1}+\sigma_y\tan\theta,\\{}_{-\theta}\sigma^{ref}_{x1}&=\sigma^{ref}_{x1}-\sigma_y\tan\theta,\\\sigma^{ref}_{x1}&=2i/\omega L_1.\end{aligned} \tag{40}$$

Since (39) is identical to the corresponding expression in (22) for $\prod_{s=1}^{2}R_s(\xi,\eta)$, but with the σ_y-*dependent* parameters ${}_{+\theta}\sigma^{ref}_{x1}$, ${}_{-\theta}\sigma^{ref}_{x1}$ replacing the σ_y-*independent* σ^{ref}_{x1}, σ^{ref}_{x2}, we have achieved our objective of implementing σ_y-*dependent* parameters. In fact, comparing the form of ${}_{+\theta}\sigma^{ref}_{x1}$, ${}_{-\theta}\sigma^{ref}_{x1}$ to the linear form we started with, $\sigma_{xo}\pm(\tan\theta)\sigma_y$, we notice that $\sigma_{xo}=\sigma^{ref}_{x1}$. Hence the steps in (31) can directly be used to calculate the PMDL layer lengths $L_1=2i/\omega\sigma^{ref}_{x1}=2i/\omega\sigma_{xo}$ and the angle of stretch θ.

The implication of (39) is shown in Fig. 7; note that $L'_j=L_j/\cos\theta_j=2i/(\omega\sigma_{xo,j}\cos\theta_j)$, where the jth pair $(\sigma_{xo,j},\theta_j)$ is obtained using (31) for the jth choice of $\sigma^*_{y,j}\in[\sigma_{y0},\sigma_{y1}]$. To summarize, an unusual mesh stretching involving groups of two layers each, with each group having $\pm\theta_j$ stretching and identical lengths, is equivalent to a PMDL whose parameters are linearly dependent on σ_y. It should be noted that the above does *not* hold if either the two lengths are different, or the stretches are not in $+\theta_j,-\theta_j$ pairs. A valid $2\times n$-layer PMDL mesh is shown in Fig. 7.

The standard PMDL formulation (with wavenumber independent parameters) is known to be applicable to convex polygonal corners [45] with the corner PMDL mesh obtained as a tensor product of the PMDLs from the two straight edges meeting

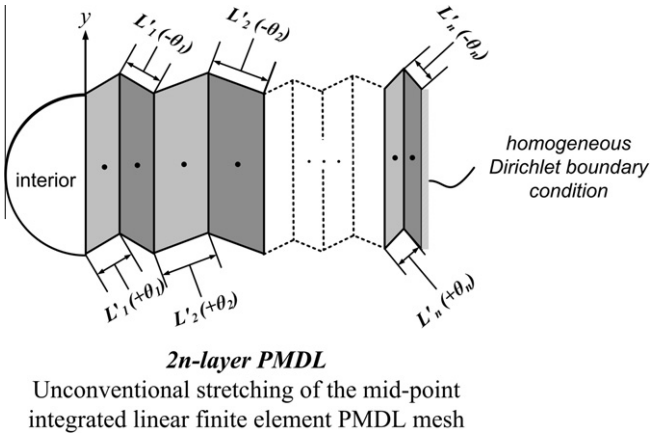

Fig. 7. The unconventional stretching of the PMDL mesh. The two layers in each 2-layer group have the same length with the stretch angles being equal in magnitude but opposite in sign.

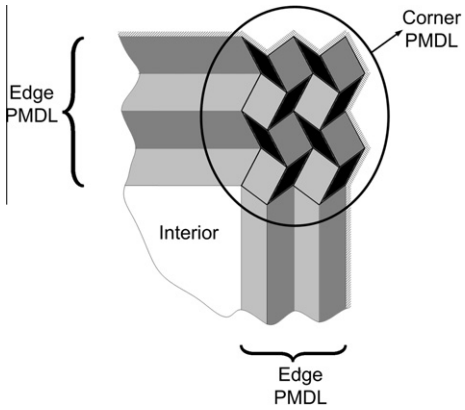

Fig. 8. The unconventional stretching of the PMDL mesh for the two orthogonal edges leads to an unconventional corner implementation.

at the corner. Analogously, we can obtain a corner mesh consistent with the above as a tensor product of two stretched PMDL meshes. Such a corner implementation for an orthogonal corner is shown in Fig. 8 and it inherits its parameters (L_j, θ_j) from the corresponding edge PMDLs.

6. Numerical experiments

Using material parameters, $c_p = \sqrt{20},\ c_s = 2,\ \varepsilon = -0.4,\ \delta = -0.1934$ and $\beta = 0$ (Type III material of [34]), we present slowness diagrams and numerical simulations to illustrate the effectiveness of the proposed method. For the purpose of numerical experiments (Sections 6.1 and 6.2) we use meshes in which all layers have identical lengths and identical magnitude of stretch angles i.e. each mesh is defined by a single pair of parameters (L, θ) or equivalently (σ_{xo}, θ); we thus drop the subscript 'j' in $L_j,\ \theta_j,\ L'_j,\ \sigma_{xo,j},\ \sigma^*_{y,j}$.

6.1. Slowness diagrams

For the material parameters chosen above, we get numerically, $\sigma_{y0} = 0.22361,\ \sigma_{y1} = 0.50000,\ \sigma_{y2} = 0.74538$ and $\sigma_{x1}|_{\sigma_y = \pm\sigma_{y2}} = 0.93752$. Using these values in (31), we get e.g. $\sigma^*_y = 0.3 \Rightarrow (\sigma_{xo}, \theta) = (0.4122, 53.95^o), \sigma^*_y = 0.4 \Rightarrow (\sigma_{xo}, \theta) = (0.5962, 56.14^o)$ and $\sigma^*_y = 0.5 \Rightarrow (\sigma_{xo}, \theta) = (0.8480, 59.48^o)$. Choosing arbitrary values of σ_{xo} and θ that violate (31) lead to inaccuracies, e.g. we can choose $(\sigma_{xo}, \theta) = (0.4122, 0^o), (1.0, 53.95^o)$. Or we could choose $\sigma^*_y \notin [\sigma_{y0}, \sigma_{y1}]$ in (31) e.g. $\sigma^*_y = 0.65 \Rightarrow (\sigma_{xo}, \theta) = (1.6704, 68.74^o)$. The resulting slowness curves are shown in Figs. 9 and 10. These figures show the exact horizontal slowness alongside the various approximate slownesses obtained using a 10-layer PMDL (2×5 layer PMDL to be precise) with varied parameters. Each plot contains the exact full-space slowness in the background (thin line) that is a combination of both the outgoing and incoming slownesses. The leftmost plot in both Figs. 9 and 10 shows the exact outgoing slownesses that need to be captured (thick line) – the remaining thin line that is visible represents the incoming slownesses. Remembering that the goal here is to approximate *all* of the outgoing slownesses related to propagating

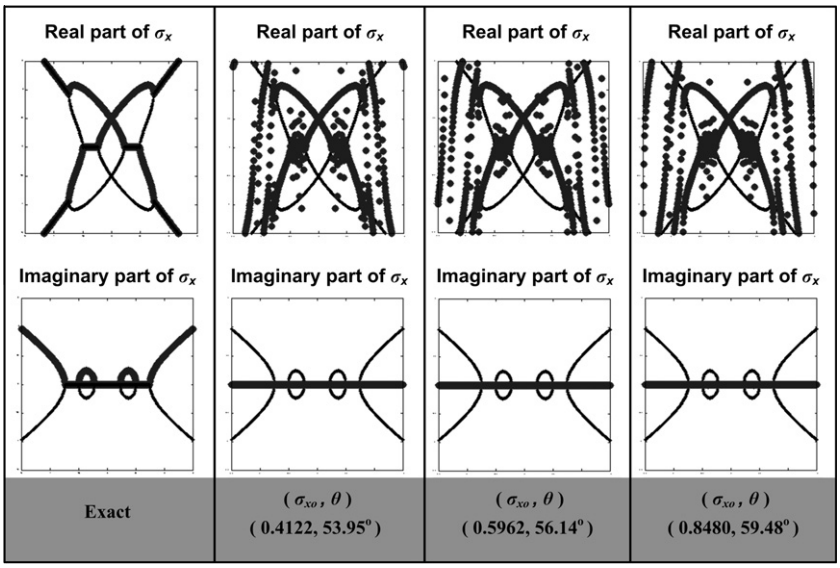

Fig. 9. Exact outgoing slowness diagram followed by 10-layer PMDL (2×5 layer grouping) slowness diagrams resulting from three different choices of parameters that all satisfy the accuracy criteria derived in this paper for treating propagating wavemodes.

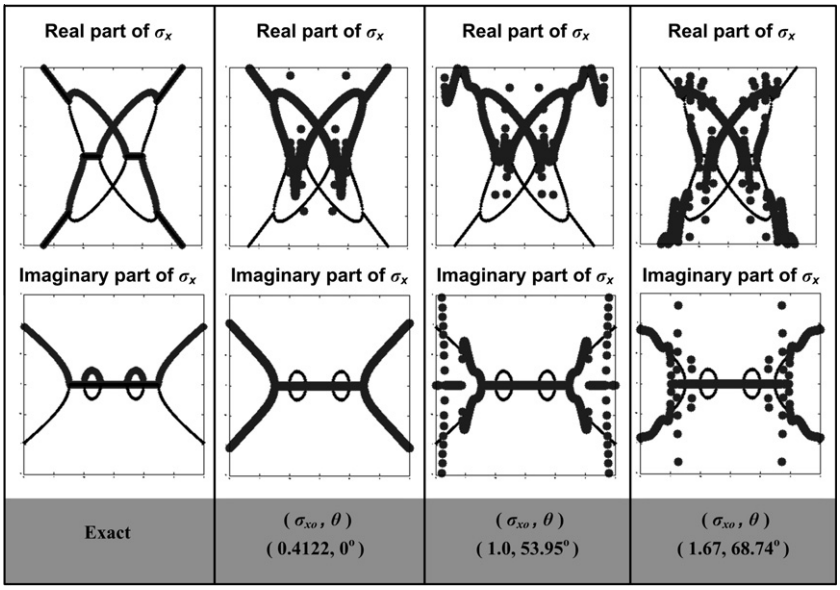

Fig. 10. Exact outgoing slowness diagram followed by 10-layer PMDL (2×5 layer grouping) slowness diagrams resulting from three different choices of parameters that violate at least one of the accuracy criteria derived in this paper for treating propagating wavemodes.

waves while capturing *none* of the incoming ones (those having non-positive group velocities), we can see that all the plots in Fig. 9 attain this goal. Of course, all the parameter choices in Fig. 9 satisfy the sufficient conditions for accuracy of propagating wavemodes and thus accuracy in the sense of (19) is guaranteed i.e. the PMDL with these parameters will converge to the exact ABC as the number of layers is increased. While the real part of the correct slowness branch is captured rather closely, the imaginary part of the slowness diagram is not approximated well. This is not surprising since we used only real PMDL parameters that are known in general to be effective against treating propagating wavemodes only [17]. Fig. 10 on the other hand shows slowness curves for parameters that do not satisfy the criterion for accuracy specified in this paper; these approximations are clearly inaccurate for propagating modes (they capture the incoming – negative group velocity branches). Moreover, the inaccuracies in approximating the imaginary parts of the slownesses is much worse in these cases compared to those in Fig. 9. While the imaginary part of the slowness approximations are zero in Fig. 9, those in Fig. 10 have negative signs. The amplitude of a wavemode with negative imaginary slowness grows exponentially in the exterior layers,

making absorption unlikely. We also mention that these inaccuracies cannot be eliminated by increasing the number of PMDL layers i.e. a wrong choice of PMDL parameters will prevent convergence to the exact solution even in the limit of a large number of PMDL layers.

6.2. Numerical simulations

We consider a 2D model problem with a rectangular interior surrounded by ABCs on all four sides and corners. The interior is modeled using regular square bilinear finite elements of size 0.05 in a grid of 60×120 elements with the four corners located at the coordinates $(\pm 3, \pm 1.5)$. The material parameters remain as $c_p = \sqrt{20},\ c_s = 2,\ \varepsilon = -0.4,\ \delta = -0.1934$ and $\beta = 0$; the frequency is assumed to be $\omega = 5$; and a localized Gaussian excitation centered at $(-1, -0.25)$ is applied along u_x as nodal excitations of amplitude $e^{-(\pi r/4h)^2}$ at each of the $5 \times 5 = 25$ nodes on a square grid of side $4h$, where h is the element length and r is

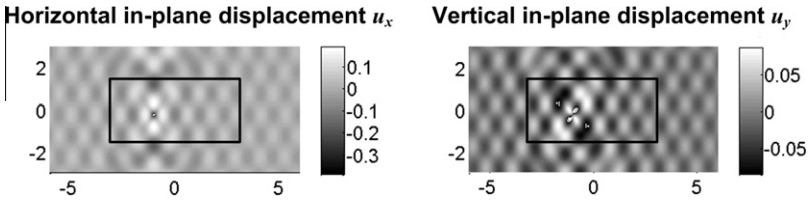

Fig. 11. Reference solution is obtained using an interior that is twice that of the computational domain marked by a rectangle. The exterior is made of 4 padding layers followed by a 20-layer PMDL (2×10 layer grouping). The excitation is a localized Gaussian along u_x.

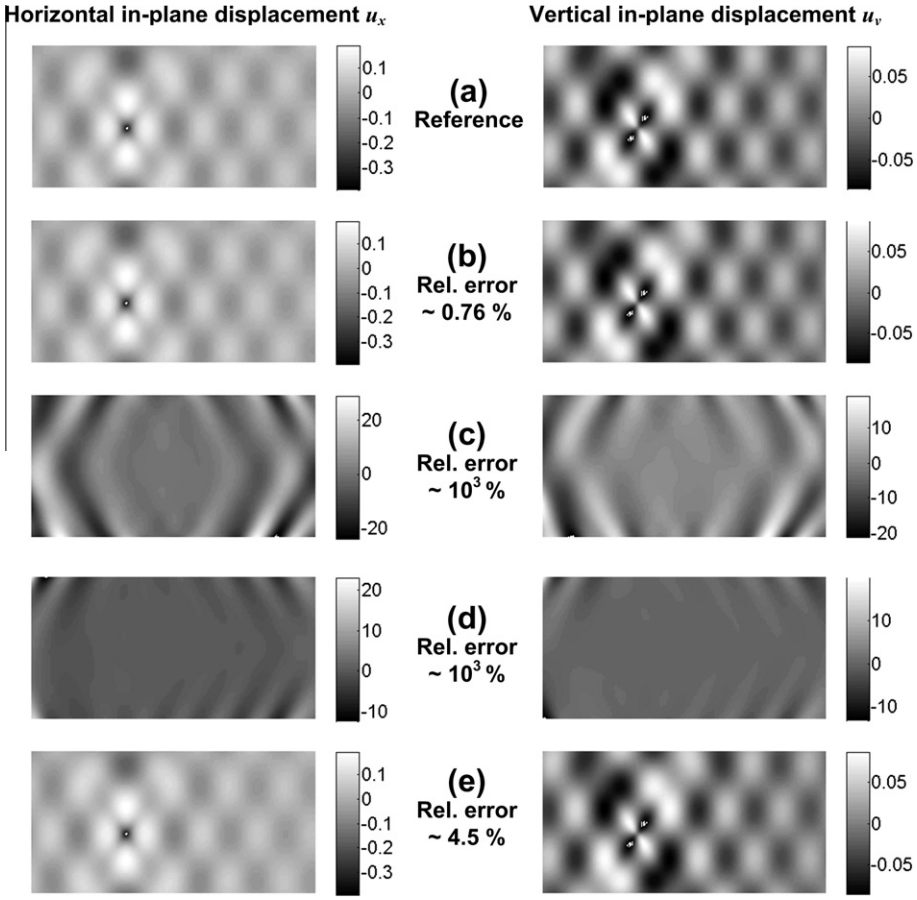

Fig. 12. (a) Reference solution obtained with twice the interior shown and a reference exterior. Cases (b)–(e): Interior solution with percentage relative error for various choices of exteriors. The exteriors used in cases (b), (c) and (d) have 4 padding layers while case (e) has none. All cases (b)–(e) have a 10-layer PMDL grouped as 2×5 layers with the following parameters: Case (b) and (e) use $(\sigma_{xo}, \theta) = (0.4122, 53.95^o),\ (\sigma_{yo}, \theta) = (0.3344, 33.77^o)$; case (c) has $(\sigma_{xo}, \theta) = (0.4122, 0^o),\ (\sigma_{yo}, \theta) = (0.3344, 0^o)$; and case (d) uses $(\sigma_{xo}, \theta) = (1.0, 53.95^o),\ (\sigma_{yo}, \theta) = (1.0, 33.77^o)$.

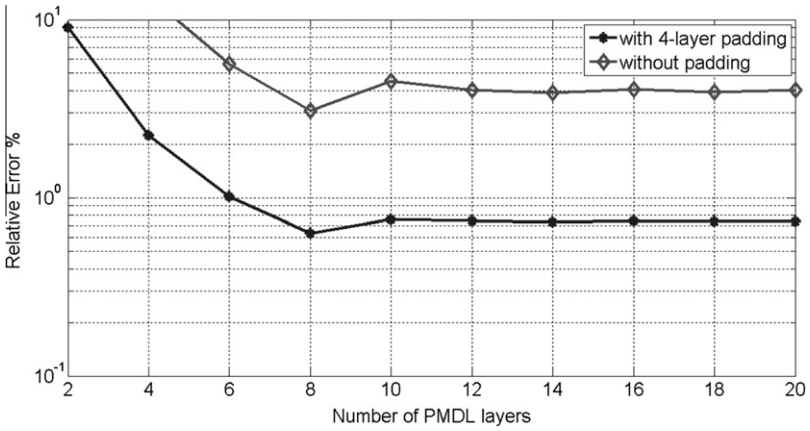

Fig. 13. Percentage relative error as a function of number of PMDL layers with and without padding. In terms of layer groupings, the *x*-axis can be read as 2×1, $2\times 2,\ldots$, 2×10 layers. The parameters used are $(\sigma_{xo},\theta)=(0.4122,53.95^o)$, $(\sigma_{yo},\theta)=(0.3344,33.77^o)$. In either case, there is convergence with increasing number of PMDL layers. The limiting error of ~4% achieved in simulations without padding is attributed to the error due to interior discretization and the error due to non-absorption of outgoing non-propagating wavemodes. The limiting error of ~0.75% in simulations with 4-layer padding is the interior discretization error.

the radial distance from the excitation center. From the previous subsection we know that a choice of $(\sigma_{xo},\theta)=(0.4122,53.95^o)$ satisfies the accuracy criteria for PMDL in the *x* direction (to ensure absorption along the vertical boundary). For PMDL in the *y* direction, it can be shown that $(\sigma_{yo},\theta)=(0.3344,33.77^o)$ similarly satisfies the accuracy conditions.

Before proceeding to determine the relative error in approximation, we point out that this work is limited to capturing outgoing propagating wavemodes only – the ineffectiveness with respect to approximating the evanescent modes ($\sigma_x\notin\mathbb{R}$) was clearly illustrated in the imaginary parts of the slowness diagrams in Fig. 9. Hence the total error in PMDL approximation is made up of the error in approximating the outgoing propagating wavemodes and the error in *not* capturing the outgoing evanescent wavemodes. To selectively eliminate the error related to non-propagating wavemodes, we use *padding* layers in addition to the ones discussed in this paper. Padding layers are PMDL based ABCs with frequency independent real-valued layer lengths (as opposed to the frequency dependent purely imaginary lengths $L_j=2i/\omega\sigma_{xj}^{ref}$ considered in the regular PMDL). Padding is known to absorb evanescent wavemodes *without* affecting the amplitude of the propagating wavemodes and is hence ideally suited to diminish only that part of the error which is related to non-absorption of these modes by PMDL [48]. Hence, unless otherwise mentioned, the exterior used in all subsequent simulations will include 4 padding layers (with ad hoc layer lengths of 0.5) followed by a *n*- layer PMDL.

The reference solution is obtained using an interior that is twice the size of the computational domain (120×240 elements) as shown in Fig. 11 with a *reference* exterior made of 4 padding layers and a 20-layer PMDL with the correct choice of PMDL parameters i.e. with $(\sigma_{xo},\theta)=(0.4122,53.95^o)$ and $(\sigma_{yo},\theta)=(0.3344,33.77^o)$. The relative error is calculated as $\|u_{PMDL}-u_{reference}\|_2/\|u_{reference}\|_2$ for both u_x and u_y and the maximum of the two is used as a measure of the overall error. The aim here is to achieve a relative error less than 1% (engineering accuracy) and the interior element size of 0.05 is chosen for this purpose.

Fig. 12 shows the interior solution for various PMDL parameters along with the corresponding percentage relative error. Fig. 12(b) shows an accurate solution (less than 1% relative error) and is obtained by using the parameters derived in this paper. The inaccuracies in Fig. 12(c), (d) are clearly evident; (c) uses the correct σ_{xo}, σ_{yo} with the wrong (zero) stretch angles while (d) uses the correct stretch angles with the wrong σ_{xo}, σ_{yo}. Fig. 12(e) shows the solution with the right parameters, but without the padding layers ((b), (c) and (d) all use 4 padding layers in their exterior). The increased error in (e) as compared to (b) can be attributed to the effect of evanescent modes and demonstrate the need for padding layers.

Finally, in Fig. 13, we show the convergence with increasing number of PMDL layers for the choice of $(\sigma_{xo},\theta)=(0.4122,53.95^o)$ and $(\sigma_{yo},\theta)=(0.3344,33.77^o)$. It should be kept in mind that with effective absorption of all outgoing wavemodes, the relative error is expected to tend to the interior discretization error (*not* to zero) as the number of PMDL layers is increased – this is the ~0.75% error that we see in Fig. 13 with the use of padding layers; the fact that this is only due to the interior discretization has been confirmed by noting that it reduces as expected with increasing fineness of the interior discretization. Since PMDL with the above parameters is effective in absorbing only propagating wavemodes (see Fig. 9), the larger limiting error of ~4% obtained without padding is attributed to the non-absorption of outgoing evanescent wavemodes.

7. Summary and conclusions

An accurate local ABC for the time-harmonic modeling of in-plane propagating waves in homogeneous untilted *non-elliptic* anisotropic elastic media is presented. This local ABC is based on PMDL and incorporates an unconventional stretching

of the PMDL mesh along with the concept of a two layer grouping to ensure the accurate treatment of propagating waves. The parameters of PMDL (related to its layer lengths) and the angles of stretch are required to satisfy certain conditions that are shown to be sufficient for accuracy.

By utilizing the form of the elements in the reflection matrix, we first showed that it is impossible for a traditional local ABC (PMDL with wavenumber-independent parameters) to accurately absorb all propagating modes. We then devised an accurate PMDL with parameters that depend linearly on the vertical wavenumbers; these parameters occur in pairs and need to satisfy a simple sufficient condition for accuracy. However, the wavenumber dependence of PMDL parameters cannot be directly implemented and we thus presented an unconventional stretching of the PMDL mesh that is equivalent to implementing wavenumber-dependent PMDL parameters.

This work presents, to the best of our knowledge, the *only* local ABC developed to date, whose accuracy is rigorously proven for all the propagating modes of untilted non-elliptic anisotropic elasticity. In doing so it has overcome one of the drawbacks of using simple space–time transformations to tackle the challenges associated with $c_{px}c_{gx} < 0$, namely their inapplicability to non-elliptic anisotropic media. Further research is underway to extend the current methodology to *tilted* non-elliptic anisotropic media.

Acknowledgement

This material is based upon work supported by the National Science Foundation under Grant No. DMS-1016514.

Appendix A. Appendix: perfect matching of coordinate transformations

Perfect matching implies that a forward propagating wave alone satisfies both displacement and traction continuity conditions at the computational boundary, thus resulting in no reflections. Perfect matching exists between the untransformed (x, y) and transformed (x', y') space when $x' = x/\cos\theta$ and $y' = y - x\tan\theta$.

Similar to (3), (32) admits modes of the kind $\mathbf{u}' = \mathbf{a}' e^{ik_{x'}x'}$ where the wavenumber $k_{x'}$ and mode $\mathbf{a}'$ satisfy the dispersion relation $\det(\Lambda') = 0$ and the governing equation $\Lambda'\mathbf{a}' = \mathbf{0}$ respectively with $\Lambda' \equiv \left(k_{x'}^2\mathbf{G}'_{xx} + k_{x'}k_y\left(\mathbf{G}'_{xy} + \mathbf{G}'^{T}_{xy}\right) + k_y^2\mathbf{G}'_{yy} - \omega^2\mathbf{I}\right)$. It can be seen from direct substitution that $k_{x'} = k_x\cos\theta + k_y\sin\theta$ makes $\Lambda' \equiv \Lambda^{in}$ and $\mathbf{a}' \equiv \mathbf{a}$ (where $\Lambda^{in}\mathbf{a} = \mathbf{0}$ is the untransformed governing equation); this implies displacement continuity across the computational boundary $x = 0$. The traction (7) under the transformation $k_y = k_{y'}$ and $\partial/\partial x = \left((\partial/\partial x') - ik_y\sin\theta\right)/\cos\theta$ becomes,

$$\mathbf{T}_x^{in} = -\left(\left(\frac{\mathbf{G}_{xx}}{\cos\theta}\right)\frac{\partial}{\partial x'} + ik_y\left(\mathbf{G}_{xy} - \mathbf{G}_{xx}\tan\theta\right)\right)\mathbf{u}, \tag{41}$$

which, with $\mathbf{u} = \mathbf{a}' e^{ik_{x'}x'}$, gives back (7) at the computational boundary (since $x = x' = 0$ and $\mathbf{a}' \equiv \mathbf{a}$); this implies traction continuity across the computational boundary $x = 0$.

References

[1] E.L. Lindman, Free-space boundary conditions for time dependent wave equation, J. Comput. Phys. 18 (1) (1975) 66–78.
[2] B. Engquist, A. Majda, Absorbing boundary conditions for numerical simulation of waves, Math. Comput. 31 (139) (1977) 629–651.
[3] B. Engquist, A. Majda, Radiation boundary conditions for acoustic and elastic wave calculations, Commun. Pure Appl. Math. 32 (3) (1979) 313–357.
[4] J.P. Berenger, A perfectly matched layer for the absorption of electromagnetic waves, J. Comput. Phys. 114 (2) (1994) 185–200.
[5] W.C. Chew, W.H. Weedon, A 3D perfectly matched medium from modified Maxwell's equations with stretched coordinates, Microw. Opt. Technol. Lett. 7 (13) (1994) 599–604.
[6] W.C. Chew, J.M. Jin, E. Michielssen, Complex coordinate stretching as a generalized absorbing boundary condition, Microw. Opt. Technol. Lett. 15 (6) (1997) 363–369.
[7] Z.S. Sacks, D.M. Kingsland, R. Lee, J.F. Lee, A perfectly matched anisotropic absorber for use as an absorbing boundary condition, IEEE Antennas Propag. 43 (12) (1995) 1460–1463.
[8] R.L. Higdon, Numerical absorbing boundary conditions for the wave equation, Math. Comput. 49 (179) (1987) 65–90.
[9] R.L. Higdon, Radiation boundary conditions for elastic wave propagation, SIAM J. Numer. Anal. 27 (4) (1990) 831–869.
[10] A. Bayliss, E. Turkel, Radiation boundary conditions for wave-like equations, Commun. Pure Appl. Math. 33 (6) (1980) 707–725.
[11] F.L. Teixeira, W.C. Chew, Analytical derivation of a conformal perfectly matched absorber for electromagnetic waves, Microw. Opt. Technol. Lett. 17 (4) (1998) 231–236.
[12] M. Kuzuoglu, R. Mittra, Frequency dependence of the constitutive parameters of causal perfectly matched anisotropic absorbers, IEEE Microw. Guided Wave Lett. 6 (12) (1996) 447–449.
[13] J.A. Roden, S.D. Gedney, Convolutional PML (CPML): an efficient FDTD implementation of the CFS–PML for arbitrary media, Microw. Opt. Technol. Lett. 27 (5) (2000) 334–339.
[14] K.C. Meza-Fajardo, A.S. Papageorgiou, A nonconvolutional, split-field, perfectly matched layer for wave propagation in isotropic and anisotropic elastic media: stability analysis, B. Seismol. Soc. Am. 98 (4) (2008) 1811–1836.
[15] D. Appelo, T. Hagstrom, G. Kreiss, Perfectly matched layers for hyperbolic systems: general formulation, well-posedness, and stability, SIAM J. Appl. Math. 67 (1) (2006) 1–23.
[16] M.N. Guddati, J.L. Tassoulas, Continued-fraction absorbing boundary conditions for the wave equation, J. Comput. Acoust. 8 (1) (2000) 139–156.
[17] M.N. Guddati, Arbitrarily wide-angle wave equations for complex media, Comput. Methods Appl. Mech. Eng. 195 (1–3) (2006) 65–93.
[18] D. Givoli, High-order local non-reflecting boundary conditions: a review, Wave Motion 39 (4) (2004) 319–326.
[19] E. Becache, D. Givoli, T. Hagstrom, High-order absorbing boundary conditions for anisotropic and convective wave equations, J. Comput. Phys. 229 (4) (2010) 1099–1129.
[20] D. Givoli, B. Neta, High-order non-reflecting boundary scheme for time-dependent waves, J. Comput. Phys. 186 (1) (2003) 24–46.
[21] T. Hagstrom, T. Warburton, A new auxiliary variable formulation of high-order local radiation boundary conditions: corner compatibility conditions and extensions to first-order systems, Wave Motion 39 (4) (2004) 327–338.

[22] S. Asvadurov, V. Druskin, M.N. Guddati, L. Knizhnerman, On optimal finite-difference approximation of PML, SIAM J. Numer. Anal. 41 (1) (2003) 287–305.
[23] M.N. Guddati, K.W. Lim, M.A. Zahid, Perfectly matched discrete layers for unbounded domain modeling, in: F. Magoulès (Ed.), Computational Methods for Acoustics Problems, Saxe-Coburg Publications, 2008, pp. 69–98.
[24] S. Savadatti, M.N. Guddati, Absorbing boundary conditions for scalar waves in anisotropic media. Part 1: Time harmonic modeling, J. Comput. Phys. 229 (19) (2010) 6696–6714.
[25] S. Savadatti, M.N. Guddati, Absorbing boundary conditions for scalar waves in anisotropic media. Part 2: Time-dependent modeling, J. Comput. Phys. 229 (18) (2010) 6644–6662.
[26] S. Savadatti, M.N. Guddati, Accurate absorbing boundary conditions for anisotropic elastic media. Part 1: Elliptic anisotropy, J. Comput. Phys. (2012), http://dx.doi.org/10.1016/j.jcp.2012.02.033
[27] F.Q. Hu, Development of PML absorbing boundary conditions for computational aeroacoustics: a progress review, Comput. Fluids 37 (4) (2008) 336–348.
[28] J. Diaz, P. Joly, A time domain analysis of PML models in acoustics, Comput. Methods Appl. Mech. Eng. 195 (29–32) (2006) 3820–3853.
[29] S. Abarbanel, D. Gottlieb, J.S. Hesthaven, Well-posed perfectly matched layers for advective acoustics, J. Comput. Phys. 154 (2) (1999) 266–283.
[30] F.Q. Hu, A stable, perfectly matched layer for linearized Euler equations in unsplit physical variables, J. Comput. Phys. 173 (2) (2001) 455–480.
[31] C.K.W. Tam, L. Auriault, F. Cambuli, Perfectly matched layer as an absorbing boundary condition for the linearized Euler equations in open and ducted domains, J. Comput. Phys. 144 (1) (1998) 213–234.
[32] E. Turkel, A. Yefet, Absorbing PML boundary layers for wave-like equations, Appl. Numer. Math. 27 (4) (1998) 533–557.
[33] T. Hagstrom, A new construction of perfectly matched layers for hyperbolic systems with applications to the linearized Euler equations, in: G. Cohen et al. (Ed.), Mathematical and numerical aspects of wave propagation, Proceedings Waves 2003, Springer-Verlag, 2003, pp. 125–129.
[34] E. Becache, S. Fauqueux, P. Joly, Stability of perfectly matched layers, group velocities and anisotropic waves, J. Comput. Phys. 188 (2) (2003) 399–433.
[35] E. Becache, A.S. Bonnet-Ben Dhia, G. Legendre, Perfectly matched layers for the convected Helmholtz equation, SIAM J. Numer. Anal. 42 (1) (2004) 409–433.
[36] F.Q. Hu, A perfectly matched layer absorbing boundary condition for linearized Euler equations with a non-uniform mean flow, J. Comput. Phys. 208 (2) (2005) 469–492.
[37] E. Becache, A.S.B.B. Dhia, G. Legendre, Perfectly matched layers for time-harmonic acoustics in the presence of a uniform flow, SIAM J. Numer. Anal. 44 (3) (2006) 1191–1217.
[38] S. Parrish, F.Q. Hu, PML absorbing boundary conditions for the linearized and nonlinear Euler equations in the case of oblique mean flow, Int. J. Numer. Methods Heat Fluid Flow 60 (5) (2009) 565–589.
[39] S. Operto, J. Virieux, A. Ribodetti, J. Anderson, Finite-difference frequency-domain modeling of viscoacoustic wave propagation in 2D tilted transversely isotropic (TTI) media, Geophysics 74 (5) (2009) T75–T95.
[40] E.A. Skelton, S.D.M. Adams, R.V. Craster, Guided elastic waves and perfectly matched layers, Wave Motion 44 (7–8) (2007) 573–592.
[41] D. Appelo, G. Kreiss, A new absorbing layer for elastic waves, J. Comput. Phys. 215 (2) (2006) 642–660.
[42] D. Appelo, T. Colonius, A high-order super-grid-scale absorbing layer and its application to linear hyperbolic systems, J. Comput. Phys. 228 (11) (2009) 4200–4217.
[43] V. Lisitsa, E. Lys, Reflectionless truncation of target area for axially symmetric anisotropic elasticity, J. Comput. Appl. Math. 234 (6) (2010) 1803–1809.
[44] I.L. Sofronov, N.A. Zaitsev, Transparent boundary conditions for the elastic waves in anisotropic media, in: S. Benzoni-Gavage, D. Serre (Eds.), Hyperbolic Problems: Theory, Numerics, Applications, Springer, Berlin, Heidelberg, 2008, pp. 997–1004.
[45] M.N. Guddati, K.W. Lim, Continued fraction absorbing boundary conditions for convex polygonal domains, Int. J. Numer. Methods Eng. 66 (6) (2006) 949–977.
[46] L. Thomsen, Weak elastic anisotropy, Geophysics 51 (10) (1986) 1954–1966.
[47] T. Hagstrom, T. Warburton, Complete radiation boundary conditions: minimizing the long time error growth of local methods, SIAM J. Numer. Anal. 47 (5) (2009) 3678–3704.
[48] M.A. Zahid, M.N. Guddati, Padded continued fraction absorbing boundary conditions for dispersive waves, Comput. Methods Appl. Mech. Eng. 195 (29–32) (2006) 3797–3819.